Guilherme Cadete Paixão da Costa

Licenciatura em Engenharia de Materiais

3D Printed Graphene Based Supercapacitors

Dissertação para obtenção do Grau de Mestre em
Engenharia de Materiais

Orientador: Professora Doutora Isabel Mercês Ferreira, Professora Associada, FCT-UNL

Júri:

Presidente: Doutor João Paulo Miranda Ribeiro Borges

Arguentes: Doutora Ana Catarina Bernardino Baptista

Setembro de 2019

FACULDADE DE
CIÊNCIAS E TECNOLOGIA
UNIVERSIDADE NOVA DE LISBOA

3D Printed Graphene Based Supercapacitors

Dedicado aos meus pais, que me deram liberdade para crescer

Agradecimentos

Gostaria de começar por agradecer à Professora Dra. Isabel Ferreira, que me orientou a tese e sempre se demonstrou recetível e disponível para todas as minhas dúvidas e ideias, fomentando sempre a procura de respostas através da experimentação.

Um especial agradecimento ao Nuno Lima, que aturou todos os meus brainstorms contribuindo com ideias que levaram à progressão deste trabalho de uma forma bem mais eficiente.

Não posso deixar de agradecer a todos os membros da equipa da Professora Isabel, que se mostraram sempre disponíveis a acompanhar-me e ensinar-me procedimentos que nunca tinha feito. Sem vocês isto não tinha corrido tão bem.

Obrigado ao professor Rui Silva que no decorrer do curso sempre estabeleceu qual o perfil que um engenheiro deve ter, dando o exemplo. Obrigado por estar sempre disponível para ensinar.

Além, Dias, Carrelo, joseph, JP, Moniz, Magda, Moura e Fred obrigado por fazerem destes anos de faculdade dos melhores da minha vida.

Ao concilio, um obrigado por me aturarem todos estes anos.

À minha namorada Inês, obrigado por tudo.

Obrigado aos meus pais por sempre me darem a liberdade para crescer e por me proporcionarem as experiências mais importantes que tive, ao meu irmão por não me ter agradecido na tese dele.

Por fim, à minha avó, que sempre incentivou os netos para sonharem.

Este trabalho teve o apoio financeiro dos seguintes projectos: ERC-CoG-2014, CapTherPV, 647596; ERC-POC-2019,CAPSEL, 855018 e UID/CTM/50025/2019.

Abstract

This thesis aims to develop graphene-based supercapacitors. There is an emerging interest in the development of lightweight, high capacity and high durability supercapacitors. As the electronic equipment are getting lighter and lighter but simultaneously requiring more power supply, the energy density of batteries and/or supercapacitors should respond to this demand. Therefore, graphene-based supercapacitors have been investigated as potential material for high capacity power sources. The graphene is a very light material and has a huge surface area together with high conductivity, thus it is ideal for charge accumulation.

In this work graphene was obtained by electrochemical exfoliation as a greener and harmless technique when compared to Hummer's method. Two rods of graphite we used as electrodes for electrochemical exfoliation in a bath of H_2SO_4 , being studied the influence of acid concentration and applied potential on the graphite/graphene powder quality. That was evaluated by XRD, SEM and micro Raman spectroscopy.

The obtained graphene-oxide powder was mixed with a polymeric binder agent and then used to print electrodes. The conductive of electrodes was optimized with a thermal treatment around 350ºC in different atmospheres. The performances of supercapacitors were tested for two different geometries, vertical (sandwich type) and planar (inter-digital configuration). These devices were studied for their stability and capacitance by CV curves and electrochemical impedance spectroscopy.

This work proves that it is possible to use graphene-oxide powder, produced via electrochemical exfoliation, to make 3D printable inks for supercapacitors applications.

Key words: Supercapacitors, 3D printing, graphene-oxide, electrochemical exfoliation.

Resumo

Esta tese tem como objetivo desenvolver supercondensadores baseados em grafeno. O interesse no desenvolvimento de supercondensadores leves, com elevada capacidade e estabilidade tem emergido nos últimos anos. À medida que os equipamentos eletrónicos ficam cada vez mais leves e cresce também a sua necessidade de consumo de energia, dispositivos como os supercondensadores podem dar resposta a esta necessidade. Portanto, os supercondensadores à base de grafeno têm vindo a ser investigados como material promissor para aplicações em fontes de energia de alta capacidade. O grafeno é um material extremamente leve com uma enorme área superficial, combinada com uma elevada condutividade, sendo por isso ideal para acumulação de cargas.

Neste trabalho, o grafeno foi obtido por exfoliação eletroquímica por ser uma técnica mais ecológica e menos perigosa quando comparada com o método de Hummer. Duas barras de grafite foram usadas como elétrodos num banho de H_2SO_4 e foi estudada a influência da concentração de ácido e do potencial aplicado na qualidade do pó grafite/grafeno obtido. DRX, SEM e espetroscopia de micro Raman foram as técnicas de caracterização utlizadas para avaliar a qualidade do material.

O pó de óxido de grafeno obtido foi misturado com um ligante polimérico a usado para imprimir elétrodos. A condutividade dos elétrodos foi otimizada com tratamento térmico a 350°C em diferentes atmosferas. O desempenho dos supercondensadores foi testado para duas geometrias diferentes, vertical (tipo sanduiche) e planar (configuração interdigital). A estabilidade e capacidade destes dispositivos foi estudada através de curvas CV e espetroscopia de impedância eletroquímica.

Este trabalho prova que é possível usar pó de óxido de grafeno, produzido por exfoliação eletroquímica, para fabricar pastas para impressão 3D e com elas produzir supercondensadores com qualquer geometria.

Palavras-chave: Supercondensadores, impressão 3D, oxido de grafeno, exfoliação eletroquímica

Table of contents

List of tables

List of figures

Acronyms

CV	Cyclic voltammetry
DMF	Dimethylformamide
EDLC	Electric Double Layer Capacitors
EDS	Energy-dispersive X-ray spectroscopy
EIS	Electrochemical impedance spectroscopy
ε_0	Dielectric constant of vacuum (8.85×10^{-12} F/m)
ε_r	Relative dielectric constant
GO	Graphene oxide
HOPG	Highly oriented pyrolytic graphite
M	Molar
PVA	Polyvinyl alcohol
PVDF	Polyvinylidene fluoride
rGO	Reduced graphene oxide
SEM	Scanning electron microscope
XRD	X-ray diffraction

1

1. Motivation and objectives

We live in a world where there is an increasing demand for better ways to store and transport energy. Each day more products are equipped with electronical components, and so this energy storage crisis is reaching almost every sector, from mobile phones to cars.

Supercapacitors promise to be the best option, when granting greater energy densities while preserving the power density of the conventional capacitor. Indeed, when compared to the common batteries supercapacitors can provide higher power in the same volume, but stores less amounts of charges, making it ideal for applications where high power bursts are necessary but no high energy storage capacity is needed [1].

Graphene raises as a super material related to several field of studies, from high-performance nanocomposites to electronics [2]. Possessing such fascinating properties, this material promises to transform several areas, including supercapacitors technology, thanks to its high surface area.

The principal purpose of this work is to fabricate graphene-based supercapacitors employing environmentally friendly methods for obtaining electronic quality graphene and the complete supercapacitor as well. Therefore, the work was divided in three main steps:

- Optimization of the electrochemical exfoliation for the graphene oxide powder production.
- Production of a 3D printable ink using GO powder and a polymer-based agent.
- 3D printing of an all solid-state supercapacitor.

2

2. Introduction

Supercapacitors show promising properties for being the power devices of the future applications, being the subject of several studies in the last few years [3]. In this thesis 3D printed graphene-based supercapacitors were developed and characterized.

2.1 Carbon based materials

Graphene by definition is an isolated single-atom layer of graphite where the carbon atoms are arranged in a hexagonal bi-dimensional honeycomb lattice [4]. Because of its prodigious properties, such as high surface area and high electrical conductivity, this material has proved to be a viable option for electrodes in supercapacitors [2].

The carbon atoms in the crystal lattice are connected by two different bonds, a strong one (σ bond) and a weak one (π bond). The σ bond is composed of the hybrid orbitals sp^2, which is the product of the $2p_x$ and $2p_y$ orbitals combined with the 2s orbital, granting the 6-atom cell covalent bonds between the atoms. On the other hand, the π bonds are the result of the $2p_z$ orbital of each atom mixed with the respective from the adjacent layer [5].

One of the best ways to the detect the existence or nonexistence of these bonds is Raman spectroscopy. When excited with a 532nm laser, the spectra obtained from carbon-based materials shows three main bands: D band at ~1350 cm^{-1}; G band at ~1580 cm^{-1}; and 2D band at ~2690 cm^{-1}, as seen in Figure 2.1. Distinct crystallographic proprieties can be related to each one of these bands: two primary in-plane vibrational modes are related to the D and G band, while the 2D band is related to the second-order overtone of D [4],[6].

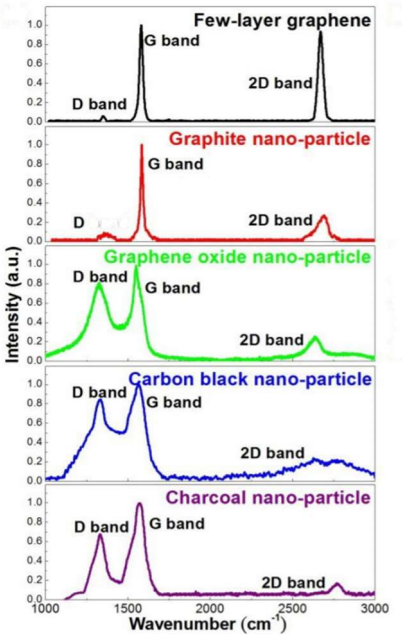

Figure 2.1 - Raman scattering spectra for different carbon-based materials. Adapted from [5]

In theory, this material has a high intrinsic mobility of 4,4 × 10^4 $cm^2 V^{-1} s^{-1}$ [7] and a specific surface area of 2630 $m^2 g^{-1}$ [8], which can only be obtained in small

samples or in specific substrates making it not available for large scale applications. But graphene alone is a material capable of a wide range of application in electronics [9]–[11].

2.1.1 Synthesis

Graphene can be synthesized through different routes, being the most used method chemical vapor deposition (CVD) [12] or mechanical exfoliation of bulk graphite [13]. Although these technics allow to obtain single-layer transferable graphene nanosheets of high purity, they show some limitations and are less adequate for large-scale applications. For industrial production of graphene-like materials the chemical synthesis route as shown to be the most promising way [8].

One way to achieve significant quantities of graphene-based single sheets is the chemical conversion of graphite into graphene oxide, and its posterior reduction [14]. The manufacturing of this material is being study for over 150 years, and since then three methods have emerged: Brodie[15], Staudenmaier[16] and Hummers method [17]. In all these three methods fuming acids are used to oxidize the graphite layers and obtain GO. With these methods it is possible to obtain a layered material of oxygenated graphene sheets with different oxygen functional groups throughout its basal planes and edges, as shown in Figure 2.2 [18]. These functional groups are responsible for the graphene's oxide hydrophilicity [19].

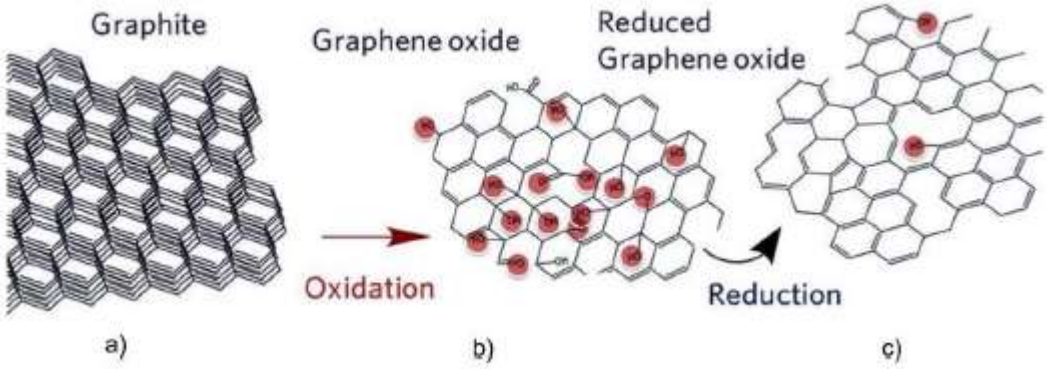

Figure 2.2 - Schematics of graphene oxide synthesis from graphite. a) Graphite structure, b) graphene oxide with highlighted functional groups and c) reduced graphene oxide with highlighted functional groups.[17]

Electrochemical exfoliation emerged as an alternative method using less aggressive agents. In this method 2 electrodes are half dipped in an electrolyte solution, being one of them a graphite rod, and a controlled potential is applied for a period of time. The electrochemical reactions occur on the external layer of the graphite electrode and detaches layers of graphite by intercalation and/or exfoliation as shown in Figure 2.3. By

varying the electrolyte solution and the electric field applied, it is possible to control the defect density, oxygen content and thickness of the exfoliated nanosheet. This process has emerged as an efficient way to produce different types of high-quality 2D nanosheets in a cost-effective way and in large scale quantities, making it ideal for energy storage and conversion, sensors and electronics applications [20], [21].

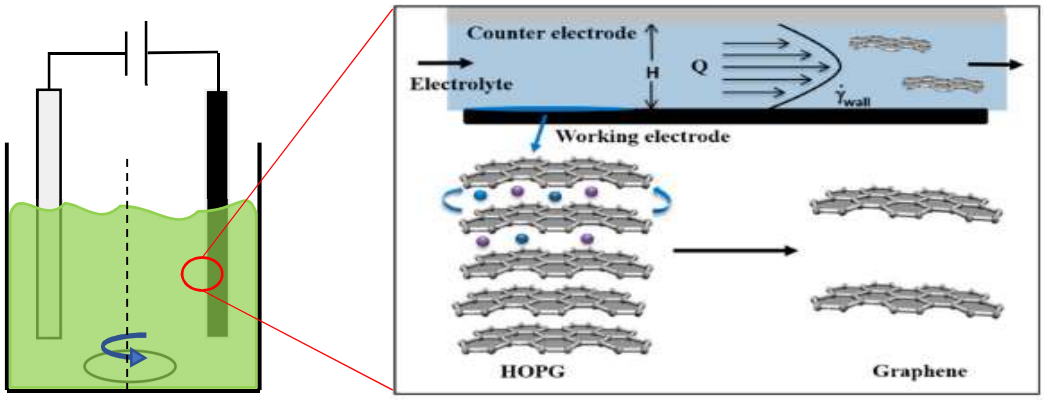

Figure 2.3 - Schematic representation of the electrochemical exfoliation mechanism on the surface of a graphite rod. Adapted from [18]

The graphene oxide obtained by electrochemical exfoliation can be reduced by different methods like photo reduction, chemical reagent reduction and thermal annealing, leading to reduced graphene oxide (rGO) [22]. The oxide functional groups from the graphene oxide surfaces are reduced by heat, causing a mass reduction of about 30% but some structural defects may affect the mechanical and electrical proprieties of rGO[23].

2.2 Supercapacitors

Capacitors are devices composed by two conducting electrodes separated by an insulating dielectric material. Charge accumulation at the electrodes happens when a potential difference is applied to the contacts of the capacitors. Energy is stored since the charges are kept apart by the dielectric layer, creating an electric field [24].

The capacitance defines the capacitor characteristics and can be calculated ratio between the stored charge, Q, and the applied voltage. The stored charge Is however, correlated with the area of each electrode, A, the permittivity of the dielectric layer, $\varepsilon_r \times \varepsilon_0$, and by the separation between electrodes, d, equivalent to the dielectric thickness in case of parallel plate capacitor[24].

$$C = \frac{Q}{V} = \frac{\varepsilon_r \varepsilon_0 A}{d} \quad (1)$$

The equation above shows that the capacitance is proportional to the area of electrodes in contact with dielectric and to be enhanced the dielectric constant needs to be very high, which is a great limitation in terms of materials that can be used, or the contact area need to increase to great extension. Therefore, a way to enhance capacitance is to use contacts with very large surface area, but as it needs to be in contact with dielectric, this must penetrate somehow into the porous electrode. Thus, liquid or low viscosity dielectric are needed. Several works have been developed In this high porosity electrodes for supercapacitors to enable them to fill the hole between the batteries and capacitors since they have specific power comparable with the one from the capacitors, while also possessing a specific energy capable of overlap some batteries [25].

The physical principles that control conventional capacitors, can be applied to supercapacitors with some adaptations. However, these devices are capable of achieving far higher capacitances by employing electrodes with much bigger surface area and thinner dielectrics [24].

Electric Double Layer Capacitors (EDLC's) are an example. The charges gathered at the surface form an electric double-layer, at both electrodes, causing an enhanced charge accumulation and consequently the capacitance of the device.

The Helmholtz model, proposed in 1853, allows to estimate the capacitance of these devices.

$$\frac{C}{A} = \frac{\varepsilon}{4\pi\delta} \quad (2)$$

Where C is the capacitance, A is the surface area, ε is the relative dielectric constant of the electrolyte and δ is the distance between the center of the ion layer and the electrode, which is usually a few Angstroms [26].

2.2.1 Electrodes

As previously noticed, the electrode surface area plays an important role in the capacitance, and so, graphene comes up as a prominent candidate as an electrode material. On account of its large surface area and 2D geometry, it can further improve the capacitance of such devices [10], [27]–[29].

2.2.2 Electrolytes

Besides the electrodes, EDLC's require an electrolyte layer between the electrodes. This component calls for specific characteristics, being the most important the ion sizes of the electrolyte. This will determine the ion's mobility and even its penetration in the

electrode's active material, which has a direct influence in the response time of the device [30].

The use of solid or gel electrolytes over liquid ones is an important development, which allows the fabrication of devices more compact, more dependable, environmentally safe and safer for the user [31]. However, the ion mobility in these sorts of electrolytes is much slower when compared to liquid ones, having a negative effect on the device's performance.

2.2.3 3D printing

3D printing is an additive manufacturing technique creates a wide range of structures and complex geometries from three-dimensional model data. In this process successive layers of material are printed on top of each other, forming a solid material. There are several methods, materials and equipment involved in 3D printing, which have been evolving over the years promising to transform manufacturing and logistics processes [32].

In the recent past, graphene oxide has shown noticeable qualities and viscoelastic properties as an aqueous dispersion where its rheological behavior is highly influenced by the graphene oxide concentration. When the dispersion has low concentration of graphene oxide, it shows a liquid-like behavior, which is not suitable for 3D printing. On the other hand, for high concentrations, the dispersion exhibits gel-like behavior with a high elastic modulus, which allows to print fine filaments or complex 3D architectures [33]. Studies show that an interdigital geometry shows the best capacitance in supercapacitors, and extruding the ink directly from the nozzle and stashing it layer-by-layer allows a high mass loading per unit area, as shown in Figure 2.4 [34]. Furthermore, the GO flakes are aligned along the extruding direction due to the shear flow conditions, enhancing the electrode's electrical conductivity [35].

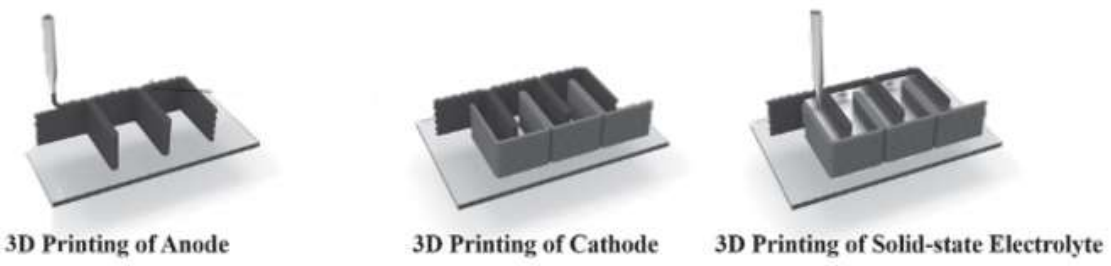

Figure 2.4 - Schematic of the 3D printed interdigitated electrodes. Adapted from [34]

3

3. Materials and methods

3.1 Production methods

The GO synthesis and electrodes formation methods are presented, and a short description of the techniques is included.

For **GO powder production**, two commercially available graphite rods were half immersed in a sulfuric acid solution with a given concentration. An electrical potential was applied to the rods for 10 minutes under heavy steering as shown in Figure 3.1. Solutions with concentrations of 0.2, 0.5 and 1 molar and electrical voltages of 5, 10 and 13V were applied in to understand the impact of this parameters in the obtained powder quality. The volume of the solutions prepared was kept constant at 100mL per cycle of 10 minutes to avoid solution saturation.

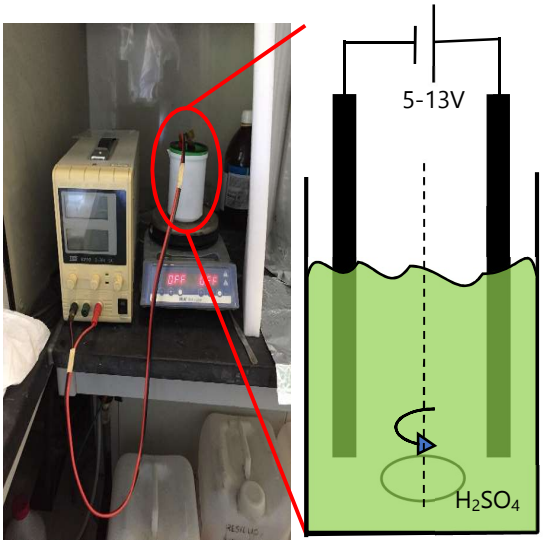

Figure 3.1 - Schematic representation of electrochemical exfoliation of graphite rods for GO production.

The product of this reaction was poured into a glass container and it was left untouched until the black powder settled. The solution was then removed carefully with a pipette. Distillated water was added to the remaining powder. This process was repeated until the solution pH was neutralized.

The container was put into an oven at 60°C until the solvent was fully evaporated, leaving only a black powder at the bottom of the container. The black powder was than stored and characterized.

The **ink** was prepared with 15mL of DMF and 1g of PVDF in a screwed flask. The solution was left under and at a temperature of 70°C until the PVDF was fully dissolved in the DMF. The flask was kept sealed to prevent DMF evaporation.

Inks with different concentrations of GO powder were produced, by adding it carefully to a solution of DMF/PVDF under steering until the powder was fully homogenized in the solution. To this mixture different concentrations of of GO powder were added: 73%, 75% or 80% together with µL of surfactant agent. The ink was then loaded into a 1mL syringe, with a 0,90 mm needle diameter.

The **electrodes geometry** designs were created using Autodesk Fusion 360, as shown in Figure 3.2. Interdigital and planar geometries were studied. The electrodes were printed using a 3D Potterbot Micro-8 adapted to fit a 1mL syringe. The printing parameters were kept constant with exception of the extrusion multiplier, which was adjusted according to the ink viscosity. Nozzle diameter was set to 0,9 mm and default printing speed to 400 mm/min, with 100% infill.

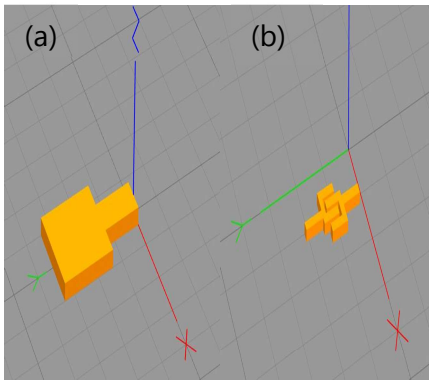

Figure 3.2 - Electrodes geometry designs studied: (a) planar, (b) interdigital

The printed pieces were then submitted to a thermal annealing at 350°C with a nitrogen atmosphere to reduce the graphene oxide.

To understand the impact the **dielectric** has on the device's capacitance, two different dielectrics were studied, one liquid and one solid. The liquid dielectric was a sweat like substance produced according to C. Callewaert and others [36].

The solid dielectric tested was a PVA|H_2SO_4 resin with a 1:1 proportion, like described by X. Ding et al [37].

Both dielectrics were deposited between the electrode's surfaces using a 1mL syringe with a 0,9mm diameter needle

3.2 Characterization

Raman spectroscopy was carried out at the materials department (FCT/UNL) using a Witec Alpha 300 confocal RAS with, equipped with a 532nm argon laser at 2mW of power. The laser beam was focused at different parts of the powder sample to access Its composition.

The surface morphology of the GO powder was obtained by scanning electron microscopy. The **SEM analysis** were made with a Phenom XL during the materiais 2019 convection.

The surface morphology and **EDS analysis** of the heat-treated printed electrodes was acquired using Scaning electron microscope Hitachi S2400 with bruker light elements EDS.

XRD analysis was used to characterize the crystalline nature and phase purity of the synthesized GO powder. An X-ray diffractometer PANalytical X'pert PRO equipped with and X'celerator detector using Cu Kα radiation at 45kV and 40mA In a Bragg-Bretano configuration was used to characterize the samples.

Small cylindrical pieces with constant diameter were produced by extruding the fabricated ink trough the nozzle of a 1mL syringe. The length of the different pieces was measured using IC Measure software. The **resistance** was then measured before and after heat treatment using a Xindar DBOL500n multimeter.

The supercapacitors fabricated were characterized in a Gamry Instruments potentiostat/Galvanostat/ZRA 3000, shown in Figure 3.3, using **cyclic voltammetry** sweeps from −0.5V to 0.5V with a step of 1mV at 9 different scan rates: 20mV/s, 40mV/s, 60mV/s, 80mV/s, 100mV/s, 200mV/s, 300mV/s, 400mV/s and 500mV/s.

EIS spectroscopy was also carried out for frequencies between 10 GHz and 10 mHz to access the equivalent circuit of the supercapacitors produced and determine the respective values.

Charge and discharge cycles were also done with a maximum charge time of 10 seconds and 1.5×10^{-4}A of charge current. All the data obtained from these characterizations techniques was processed using Gamry Echem Analyst software.

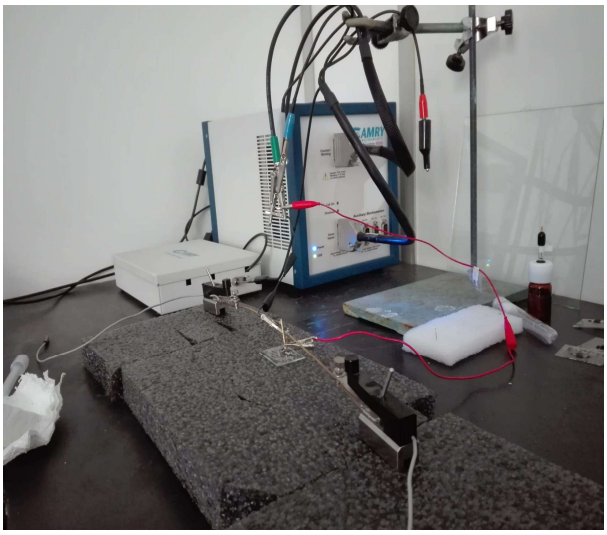

Figure 3.3 - Gamry Instruments potentiostat/Galvanostat/ZRA 3000 used to do the electrochemical characterization for this thesis

4

4. Results and discussion

In this section the results of the GO powder obtained by electrochemical exfoliation and of the supercapacitors characterization are presented and discussed.

4.1 GO powder production

GO powder can be obtained by several methods but in this thesis the electrochemical exfoliation of graphite was the one tested and used to fabricate supercapacitors. To obtain the best quality of GO powder a preliminary study had to be conducted in order to access how the electrochemical exfoliation parameters such as potential applied and electrolyte concentration influence the GO obtained.

4.1.1 Influence of the potential applied

To understand how the potential applied influences the GO powder production method, the sulfuric acid concentration of the dielectric solution was kept constant at 0.2 molar and the potential was applied for 10 minutes. The process was then carried out has described before until GO powder was obtained. Three different potentials were tested: 5V, 10V and 13V. After properly dried, each powder was weighted and analyzed with Raman spectroscopy and XRD. Table 4.1 and Figure 4.1 shows the amount of powder obtained for each potential tested, where it is possible to observe a yield gain with increasing potential. Since the distance between the electrodes was kept at (2 cm), the electric field varied according to the applied potential.

Table 4.1 - GO powder obtained mass for the different potentials tested.

Potential applied (V)	5	10	13
Obtained mass (g)	0.010	0.13	0.16

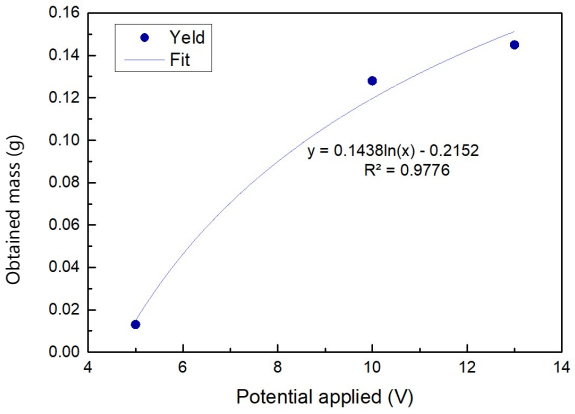

Figure 4.1 - GO powder obtained mass versus electrical potentials applied.

However, we observe a high gain when potential changes from 5V to 10V but increasing voltage above 10V does not correspond to a further significant increase in mass of GO. In this range of values, a logarithmic growth seems the empirical best match of the results. Looking at the powder obtained at this electric field, the one produced by applying 13 V, bigger agglomerates than the ones produced using lower potentials can be seen. Meaning that the electric field is enough to detach small particles of the graphite rod which is most desirable to have good quality GO with few or single foils.

To better understand how this parameter affects the powder quality and to guaranty GO powder is being produced, Raman and XRD analysis data were performed. The obtained data is plotted in Figure 4.2 and results compared to literature [38].

The Raman spectra of all three powders shows a D band (~1350 cm^{-1}), G band (~1580 cm^{-1}) and 2D band (~2690 cm^{-1}) consistency with what is found in the literature [38]. The ratio between the bands intensity however varies, implying the presence of GO with different degrees of oxidation and purity.

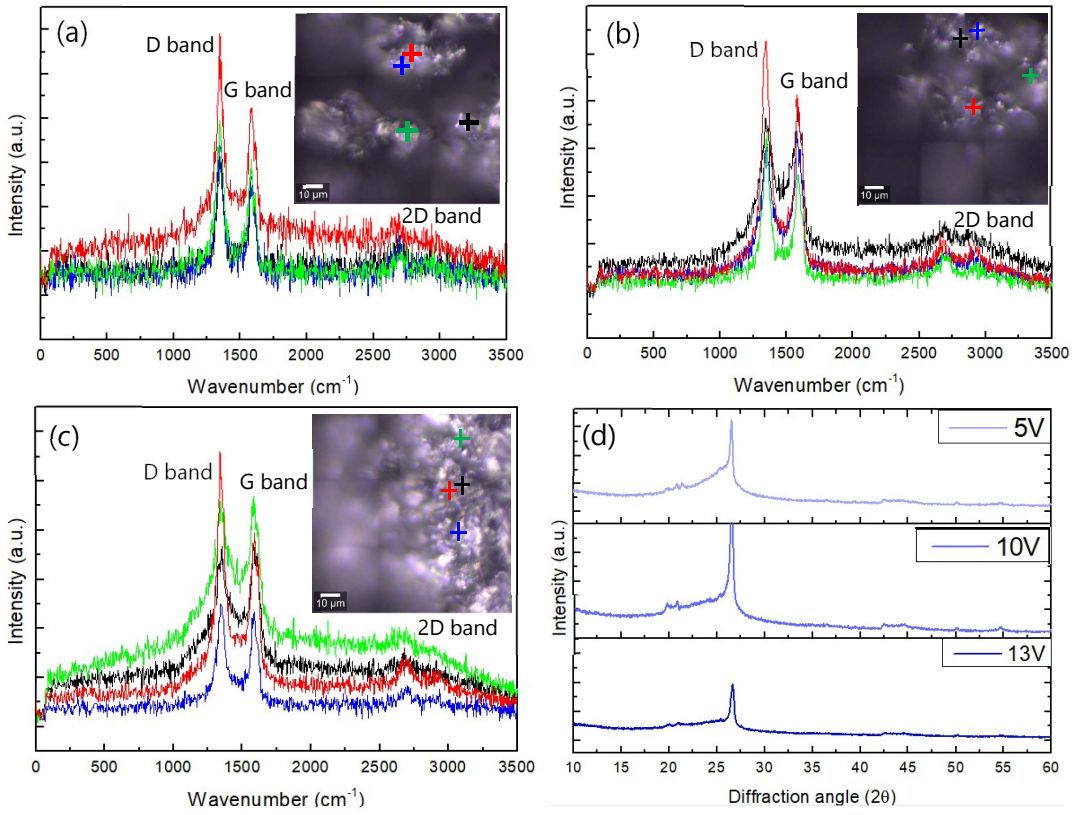

Figure 4.2 - Raman spectra of powder produced by applying (a) 5V, (b) 10V, (c) 13V and (d) the respective XRD pattern.

The XRD patterns of the different samples show a clear peak at 2θ = 26°, coherent with XRD patterns of graphite found in literature. The peak appears to get wider with decrease of the potential applied entailing an increase in the oxidation degree of the GO obtained [38].

Therefore, this study allowed to determine the best voltage, 10V, to proceed with the production of GO by this method, since the powder produced showed the second-best yielding, no big agglomerates of powder and more homogeneous Raman spectra obtained along the sample. The difference in the powder size can be observed in Figure A1 to Figure A4 in annex A.

4.1.2 Influence of the sulfuric acid concentration

The sulfuric acid solution concentration was also tested to determine how it influences the quality of the GO powder produced. To this study the potential applied was kept constant at 10V for 10 minutes. The process was then carried out as described before until GO powder was obtained. Three different concentrations were tested: 0.2M, 0.5M and 1M. After properly dried, each sample was weighted and analyzed with Raman spectroscopy and XRD. Table 4.2 and Figure 4.3 shows the amount of powder obtained for each concentration tested, where it is possible to observe a yield gain with increasing concentration. The increase in concentration also produced bigger powder agglomerates, which is not ideal for ink manufacturing and therefore should also be considered. Although an exponential increase is fitted to the experimental points in this range of concentration, excessive increase in concentration leads to enhancement of big particles in the exfoliated GO powder, again not desired for the constitution of a good ink.

Table 4.2 - GO powder obtained mass for the different sulfuric acid concentrations tested.

H_2SO_4 concentration (M)	0.2	0.5	1
Obtained mass (g)	0.13	0.16	0.26

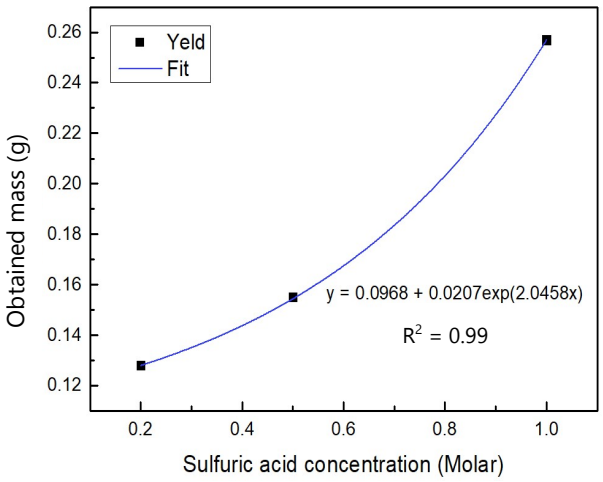

Figure 4.3 - GO powder obtained mass versus sulfuric acid concentrations tested.

The Raman spectra and XRD data were plotted in Figure 4.4 to study how the electrolyte solution concentration impacts the powder quality and assure GO powder is In fact being produced. These results were compared to results found in literature. [38]

It is possible to observe a D band (~1350 cm^{-1}), G band (~1580 cm^{-1}) and 2D band (~2690 cm^{-1}) in all three samples. The bands intensity ratio suffers a variation, which implies the presence of GO with different degrees of oxidation [38]. The peak intensities decrease as concentration increases, implying formation of less crystalline compounds.

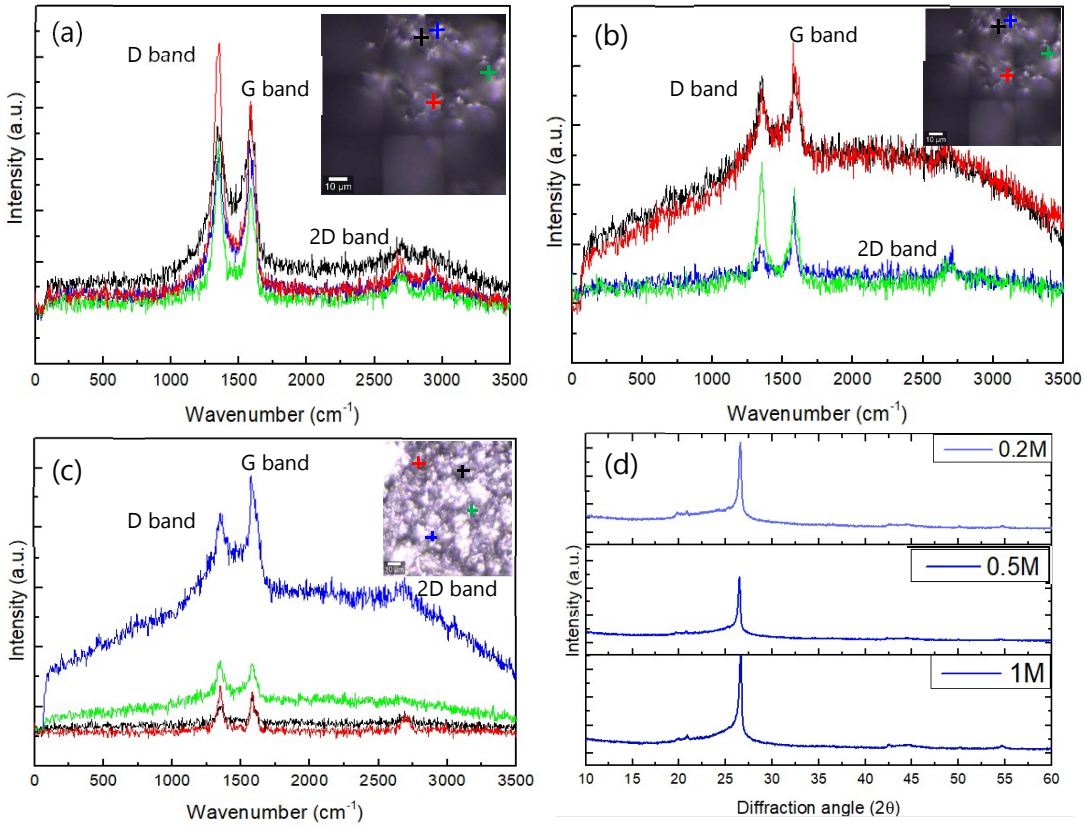

Figure 4.4 - Raman spectra of powder produced with sulfuric acid concentration of (a) 0.2M, (b) 0.5M, (c) 1MV and (d) the respective XRD pattern.

A peak located at 2θ = 26° can be observed in all the samples XRD patterns, which is coherent with XRD patterns of graphite found in literature. The patterns show little to no difference as studied concentration increases meaning this parameter has a small influence in the oxidation degree of the GO produced.

Overall, it was possible to determine that the best concentration of sulfuric acid for this process is 0.2M since it showed little difference in yielding when compared to bigger concentrations, produced thinner powder and had a more defined 2D band in the

Raman spectra along the samples. The characterized samples were composed by the full powder left in the solution, the use of only the supernatant powder can prove beneficial for the GO produced since it will be constituted of less dense particles meaning fewer layered GO. The difference in the powder size can be observed in Figure A1 to Figure A4 in annex A.

4.1.3 SEM analysis

The Figure 4.5 presents the SEM images of GO powder obtained using the best parameters values determined before, with four magnifications. The surface morphology shows formation of flack like structures (Figure 4.5 a) commonly found in exfoliated graphene like compounds. At higher magnifications it is possible to observe the bigger grains are formed by flakes (Figure 4.5 b) but further enlargement of the image reveals also few nanometer foils close to the graphite like sheets. Thus, graphene sheets are formed even though they are crumpled and forming micro-blocks of graphite. Indeed, this comes in agreement with the results obtained from Raman and XRD. From XRD only the graphite like flakes are detected while Raman also detects graphene oxide sheets.

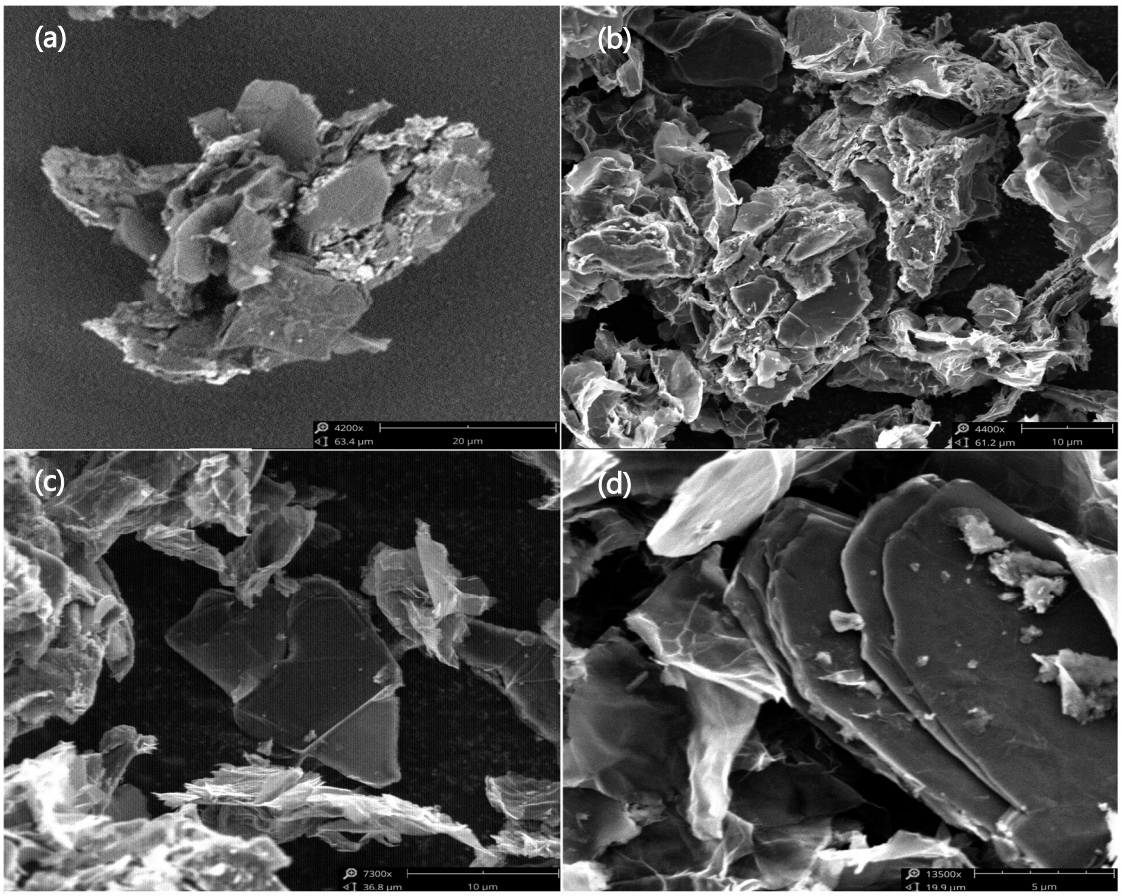

Figure 4.5 - SEM images of GO powder obtained with magnifications of (a) 4200×, (b) 4400×, (c) 7300× and (d) 13500×.

These were the expected results, since GO single foils are extremely difficult to obtain by electrochemical exfoliation.

This process proved to produce few layered graphene oxide sheets contained in the large flakes that would have high surface area and should be adequate for supercapacitors applications.

4.2 Ink production

After definition of the best electrochemical exfoliation parameters for obtaining GO sheets, the powder produced this way was used as an active ingredient in a 3D printable ink: The ink was initially composed of GO powder and a PVDF|DMF solution. To understand the impact of the GO concentration in the ink's conductivity, inks with different powder concentration were produced, heat treated, and the conductivity measured. The concentrations tested were: 73% GO, 75%GO, and 80%GO.

The heat treatment temperature and atmosphere have an influence on the ink's conductivity therefore, various heat-treating temperatures were tested on the ink with containing 73% of GO concentration under a nitrogen atmosphere.

Three different atmospheres were tested by heat treating the same ink at a temperature of 320°C in order to understand the impact this parameter has on the powder produced this way. Oxygen, vacuum and nitrogen were the different atmospheres studied.

Through the experimental work, the pieces printed with the GO powder and PVDF|DMF solution showed severe cracks as the DMF evaporated, and so there was a need to add a surfactant agent. This enable to solve the problem and further Inks were produced with a few µL of surfactant.

4.2.1 GO concentration influence

Finding the best concentration of GO in the ink fabricated is finding a balance between the best electrical conductivity and the rheological properties that make the ink printable. For this the rheological characterization was not possible due to system maintenance, but inks with different concentrations were extruded through a 1mL syringe to make small cylinder pieces, as shown in Figure 4.6, with a constant diameter which were left drying for a day. The extrusion with the syringe enables to conclude about

the possibility of printing the ink. These pieces were heat treated using a heating ramp of 5°C/min until it reached 320°C, staying for 1 hour at that temperature. The samples were then left cooling inside the oven until room temperature. The cylinders electrical resistance was measured from end to end and the electrical resistivity was calculated. The resistivity values for the samples produced with GO concentrations of 73%, 75% and 80% are shown in Table 4.3 and Figure 4.7. The ink's resistivity was calculated using the Ideal approximation for a conductive material found in literature [39].

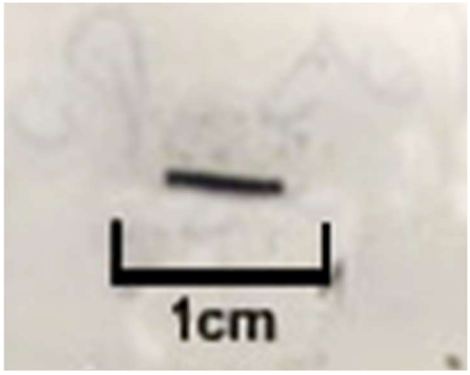

Figure 4.6 - Samples produced by extruding ink through a 1mL syringe.

There is a clear relation between the GO concentration and the ink's resistivity. As concentration increases, there is a decrease in the samples resistivity. The problem here is, as the load increases in the PVDF|DMF solution, it leads to high viscosity properties and the ink be hardly extruded through the tip 3D printing. And so, an ink produced with 80% concentration of GO provides the lowest resistivity but it is also the ink most dificult to print.

Table 4.3 - Mean resistivity of the inks produced with different GO concentration. Mean resistance calculated using values in table B1 in annex B.

GO concentration (%)	Mean resistivity (Ω.cm)	Standard deviation (Ω.cm)
73	7.6	1.3
75	4.9	1.6
80	3.4	0.20

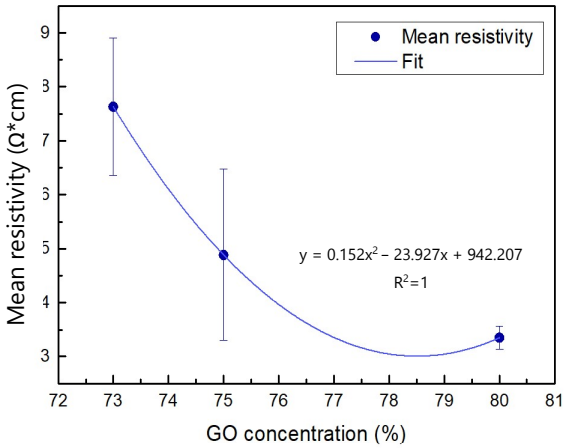

Figure 4.7 - Mean resistivity versus different GO concentration of ink.

With all this in consideration, the parameter that had finds a compromise between conductivity and rheological proprieties is the 73% of GO concentration. Although it shows the biggest resistance, which is not good for supercapacitors electrodes, it also provides less granulated ink making it more ideal for 3D printing. According to the fitting of experimental results a minimum in resistivity seems to be found at around 78%, and in further studies this should be considered.

4.2.2 Heat treatment temperature and atmosphere Influence

The heat treatment is a crucial part for printing graphene electrodes for supercapacitors since it is responsible for the GO reduction, making the ink more conductive. To study how the atmosphere of the heat treatment affects the conductivity of the samples obtained, inks produced with 73% of GO and 27% PVDF were heat treated at 320°C with three different atmospheres: oxygen, nitrogen and vacuum. The heating ramp used was 5°C/min until it reached 320°C, where it stayed for 1 hour. The samples were then left cooling inside the hoven until room temperature. The samples produced had the same geometry as the samples produced for the previous study. The resistivity of the cylinders was measured and displayed in the Table 4.4 where it is possible to observe the resistivity of the different samples analyzed.

The results obtained by the different atmospheres tested show that, heat treating with a nitrogen atmosphere produces samples with the least resistivity. It was already expected that an oxygen atmosphere would not be adequate for a thermal annealing since at high temperatures the oxygenation of the powders will increase drastically [22]. Therefore, we conclude that a reduction atmosphere Is the most proficient in reducing GO to obtain rGO.

Table 4.4 - Mean resistivity of the inks heat treated with different atmospheres. Mean resistivity calculated using values in table B2 in annex B.

Atmosphere	Mean resistivity (Ω.cm)	Standard deviation (Ω.cm)
Oxygen	55.6	4.5
Nitrogen	5.0	1.2
Vacuum	26.3	2.2

On the other hand, there was the need to understand what the temperatures impact is and see if it would be possible to obtain similar results but at lower temperatures. Thus, temperatures of 100°C, 150°C, 200°C, 270°C and 320°C were studied using a nitrogen atmosphere and processing as before. Table 4.5 and Figure 4.8 show variation on the resistivity values obtained for the different temperatures studied.

Table 4.5 - Mean resistivity of the inks heat treated at different temperatures with a nitrogen atmosphere. Mean resistivity calculated using values in table B3 in annex B.

Temperature (°C)	Mean resistivity (Ω.cm)	Standard deviation (Ω.cm)
100	353.8	2.3
150	182.1	2.4
200	54.30	1.6
270	32.50	1.9
320	5.0	1.2

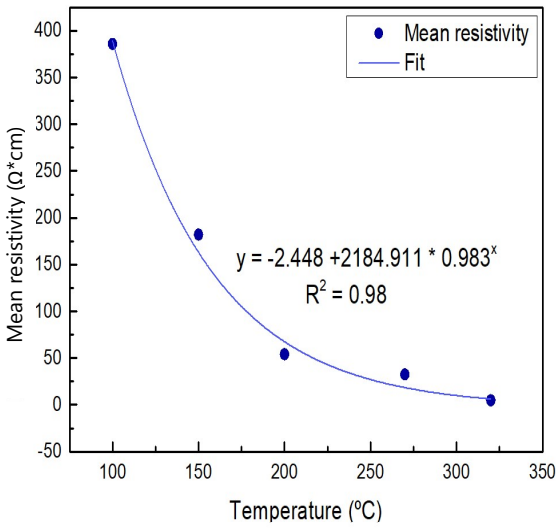

Figure 4.8 - Mean resistivity versus temperature treatment of inks in nitrogen atmosphere.

The results show that the resistivity obtained follows an exponential decay in respect to the annealing temperature increase, therefore heat treating at temperatures around 320°C proves to be the best annealing temperature. There was no interest in studying temperatures above 400°C since PVDF starts deteriorating, making the physical properties of the obtained samples not suited for these kind of applications.[40]

4.2.3 Surfactant concentration influence

As mentioned before, when the best parameters for the inks production were set and electrodes started to be printed, the pieces presented several cracks before the heat treatment. This meant that as the DMF evaporated from the samples, it left empty spaces leading to severe cracks such as the ones shown in Figure 4.9, due to non-coalescence of the GO particles.

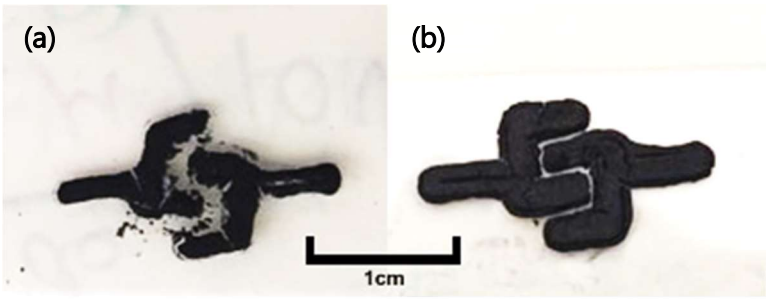

Figure 4.9 - Difference between the samples produced using ink (a) without and (b) with Surfactant.

Thus, there is a need for a surfactant in the ink to allow GO particles to be bonded and form a uniform ink without particles agglomeration. A surfactant agent helps because It has a long molecule that contributes to maintain GO particles separated. The surfactant chosen for this study was polysorbate.

In addition, the surfactant allows to increase the load of GO in the ink to 80% without compromising its rheological proprieties making it printable and led to the fabrication of electrodes with higher definition. Table 4.6 provides information about the impact of the concentration of surfactant in the ink's resistance. The inks produced had 80% of GO and 20% of PVDF, and the surfactant was added relative to the volume of PVDF|DMF solution used. The procedure for this study was the same used in previous ones, whereas here the temperature used for the thermal annealing was 340°C due to hoven overshooting.

Table 4.6 - Surfactant influence on the ink's resistivity. Mean resistivity calculated using values in table B4 in annex B.

Surfactant added (µL/mL)	Mean resistivity (Ω.cm)	Standard deviation (Ω.cm)
0	4.7	1.2
2	134.0	26.2
5	127.1	6.9
8	323.3	154.3

The addition of just 2µL of surfactant per millimeter of PVDF|DMF is enough to increase significantly the ink's resistivity by a factor of 33. To guarantee the best performance of the electrodes it is imperative they possess the lower resistivity possible, but the presence of cracks can also be a factor that can lead to a bad operation, and so it is important to find a compromise between these two factors.

The results obtained show no significant differences between adding 2µL/mL or 5 µL/mL in terms the ink's resistivity, however using 5 µL/mL resulted in samples with less

cracks. Therefore, in the capacitor devices 5 µL/mL of surfactant was used in the ink for printing the electrodes.

4.3 Printing the electrodes

Defined the best composition for the ink it was introduced in a 1mL syringe with a 0.9mm diameter needle and loaded on the 3D potter printer. The printing parameters were set by trial and error attempts until it was possible to print the desired geometries. All the values used for printing were the ones set by simplify 3D software as default for PLA filament, except the ones displayed in in table B5 in annex B

With these parameters it was possible to print both the geometries intended to be studied in this thesis. During the trial and error attempts the parameter that seemed to have a bigger influence in the printing quality were the extrusion multiplier and the default printing speed, since the first controls how much ink is extruded during the time of printing and the second controls the printers arm speed.

4.3.1 SEM/EDS characterization

The Figure 4.10 shows SEM images from the printed electrode's surface with two different magnifications. The surface seems to be composed of oriented sheet like structures, just as expected from a 3D printing extrusion method.[33] Furthermore, it is possible to observe micro grains formed by foils with empty spaces between them, meaning the structures present in the GO powder produced were conserved after heat treatment.

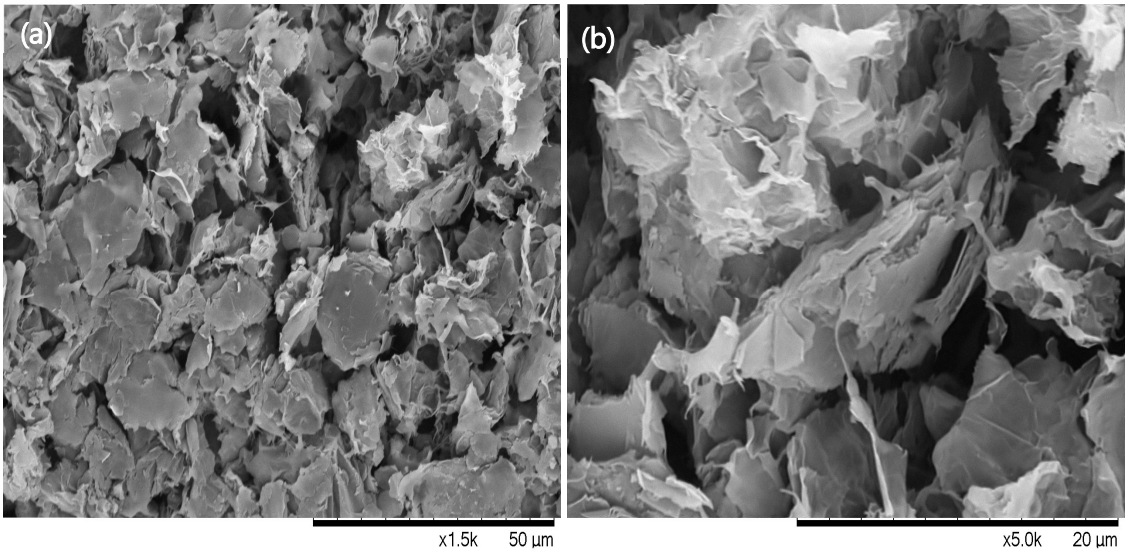

Figure 4.10 -SEM analysis of the printed electrodes surface with different magnifications (a) ×1500 and (b) ×5000.

With this SEM analysis is also possible to observe small filaments that connect the micro grains, being possibly the PVDF working as a binding agent for the GO powder. To better understand the composition of the observed structures, EDS quantification and mapping was carried out and the results can be observed in Table 4.7 and Figure 4.11.

The samples show high percentage of C and O, since GO is mainly composed by these two elements. The presence of fluorine is explained by the PVDF used as a binding agent, and it proves PVDF did not evaporate during the thermal treatment. The only element which presence cannot be explained is silicon, since it is not an element present in any of the compounds used for the fabrication of these electrodes. Its low percentage may indicate it as a contamination from other samples analyzed at the same time.

Table 4.7 - EDS quantification of the elements presents in the electrode's surface.

Element	Wt%	Atm%
Carbon	68.41	76.40
Oxygen	15.36	12.88
Fluorine	12.97	9.16
Silicon	3.27	1.65
Total	100	

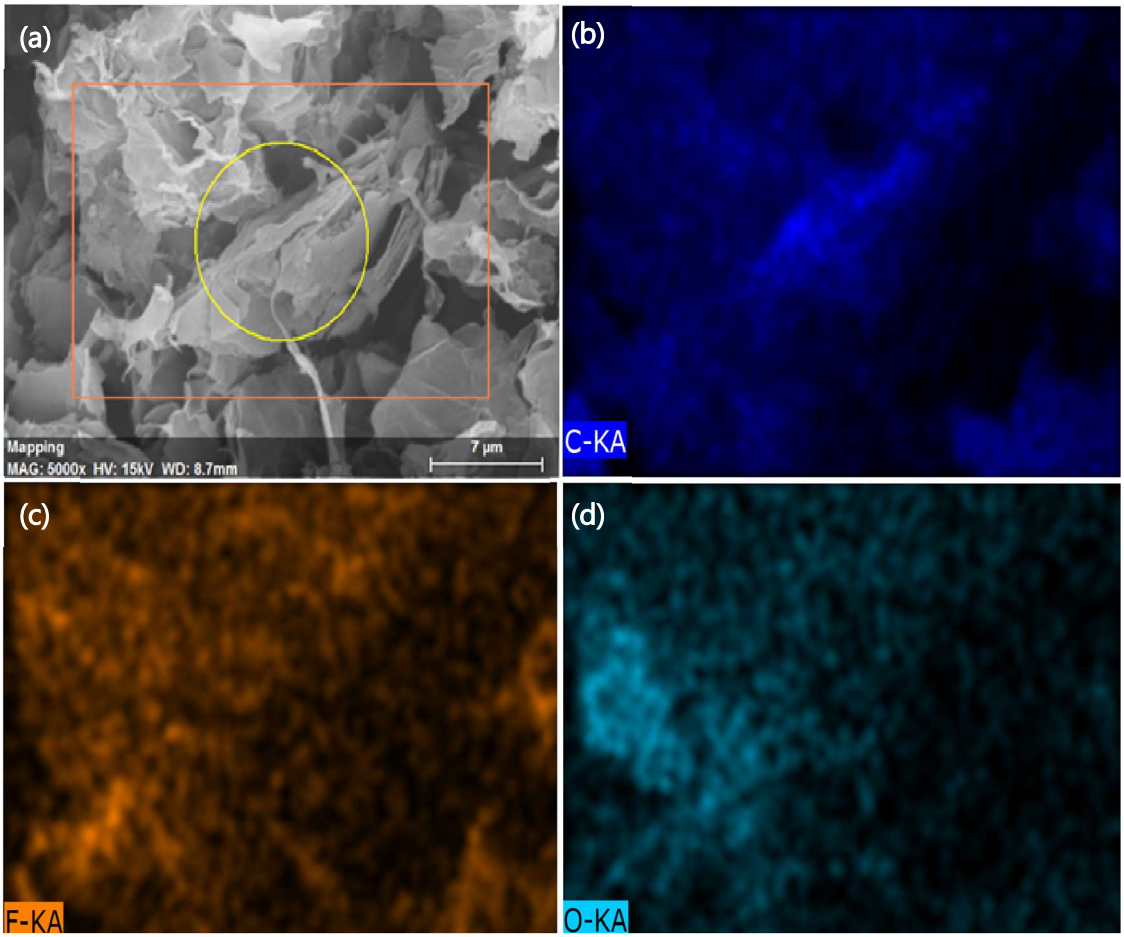

Figure 4.11 - EDS characterization of the electrode's surface in the (a) targeted area containing (b) carbon, (c) fluorine and (d) oxygen elements.

The mapping images suggest the carbon is the main constituent of the micro grains and the oxygen is filling the empty spaces around them. Fluorine appears to be spread along the grain's surface and in the spaces between them, meaning it is working as a binding agent which is what was intended for it to do.

4.4 Capacitors

With the best ink and printing parameters determined, electrodes with interdigital and planar geometries were printed and characterized. images of the electrodes printed can be seen in Figure 4.12. These geometries were chosen as a first approach to validate the 3D printing process for supercapacitor fabrication. Besides that, two different dielectrics were used for this study to understand its influence on the device's performance.

For these studies 2 planar supercapacitors and 8 interdigital were fabricated and tested to verify the reproducibility of the process. All the samples printed can be seen in Figure A5 to Figure A7 in annex A.

As the resistivity of rGO electrodes is high, there is a need to add contacts made of a more conductive material, to better collect the charges stored. For this purpose, carbon and silver inks were tested as possible contacts.

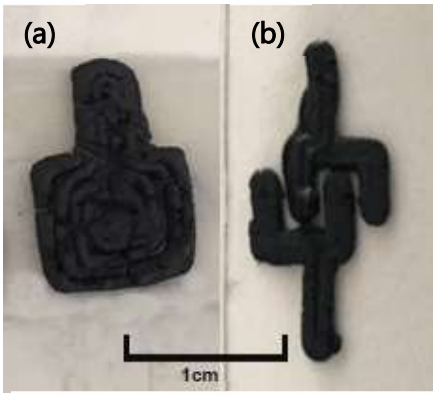

Figure 4.12 - Example of the electrode's geometries studied in this thesis. (a) planar and (b) Interdigital geometries.

4.4.1 Contacts influence.

To test how different contacts affect the devices preformance, the same device was tested without contacts, with carbon contacts and with silver contacts using a sweat simulated substance as the dielectric. 5 cycles of cyclic voltometries were performed to each contact tested, with a potential range between −0.5V and 0.5V, a scan rate of 60mV/s, Figure 4.13 shows the 5^{th} cycle for each case. The spectific capacity of the device was determined for each contact, using Gamry Echem Analyst software, and the results are displayed in Table 4.8. This study was performed on the supercapacitors with an interdigital geometry.

The results of this tests show a boost in the current when silver contacts are used for all 4 samples tested, however the metallic contact also increased the devices resistence as evidenced by the voltommetry slope. This resistance gain is probably caused by the contact interface with the GO electrode, since the carbon ink showed no slope difference when compared to the device with no contacts. Surely the increase in the corrent collection is due to lower resisntance of the silver ink so the electrical contact is better, but probably it penetrates in depth of rGO electrode reducing the interaction of the electrolyte with it so, interfaces resistance is enhanced. Due to increase of current, the capacitance is higher when compared to carbon ink or without contact, as show in Table 4.8.

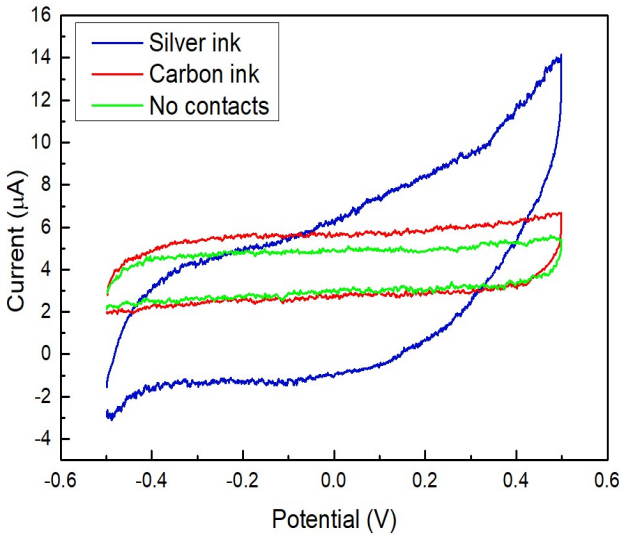

Figure 4.13 - Cyclic voltometries performed for different contacts in sample 1i with a simulated sweat substance as electrolyte.

Table 4.8 - Specific capacity of sample 1i using a simulated sweat substance as electrolyte with the different contacts.

Contact type	Specific capacity ($\mu F/cm^2$)
No contact	120.5
Carbon ink	188.1
Silver ink	458.5

Considering the contact worked better with this device was the silver one largely enhancing the devices capacitance when compared to the carbon ink.

4.4.2 Electrolyte influence

The electrolyte is an important component for the supercapacitors performance since it controls the charge accumulation due to interaction with the electrodes interface. That is reflected in the intensity of the electric field generate with consequent impact on the device's capacitance. Two electrolytes were tested PVA/H_2SO_4 and sodium chloride solution. The supercapacitors fabricated with these electrolytes were each submitted to 5 cycles of cyclic voltometries with a potential range between –0.5V and 0.5V, a scan rate of 60mV/s, and the 5th cycle of each device tested was ploted in Figure 4.14. The spectific capacity of the devices was determined using Gamry Echem Analyst software, and the results are displayed in Table 4.9. This study was only performed on the supercapacitors with an interdigital geometry.

Considering the same area of capacitor and the quantity of electrolyte added between electrodes, the cyclic voltammetry shape for the PVA/H_2SO_4 shows a higher current and more defined rectangular shape.

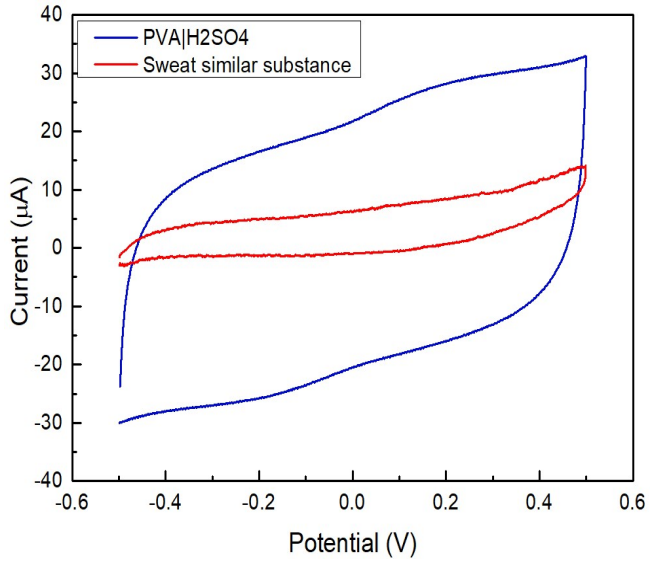

Figure 4.14 - Cyclic voltometries performed for the different electrolytes studied in samples 1i.

Table 4.9 - Specific capacity of sample 1i with different electrolytes.

Electrolyte	Specific capacity ($\mu F/cm^2$)
Sodium chloride	458.5
PVA | H_2SO_4	1759.6

The calculated device's specific capacitance value is an order of magnitude higher when using the PVA/H_2SO_4 as an electrolyte. This can be explained by the presence of a higher number of ionic molecules attracting more electrons to the surface area of the electrodes, thus higher number of charges are stored.

Electrochemical impedance spectroscopy was carried out for both electrolytes using an interdigital geometry to access the electrolyte's conductivity and the results can be observed in Figure 4.15. The conductivity variation with frequency from all the samples can be found in Figure C1 to Figure C2 in annex C.

The sweat simulated substance displays lower conductivity values when compared to the PVA/H_2SO_4 electrolyte, however this difference gets smaller as frequency increases. Both electrolytes display conductivities between 10^{-7} S/cm and 10^{-3} S/cm for high frequencies, which is within the desirable values for electrolyte conductivity [41].

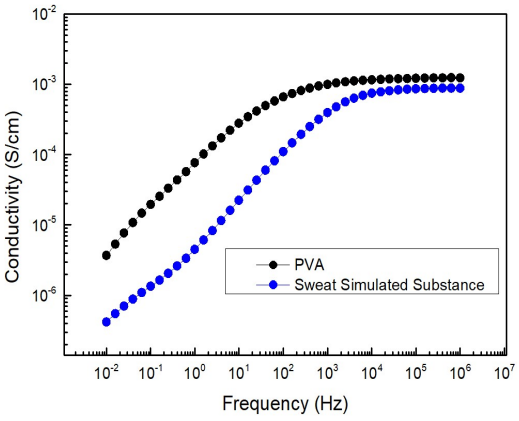

Figure 4.15 - Electrical conductivity variation with frequency for sample 6i.

The liquid electrolyte proved to be harder to deposit than the solid one, due to the electrode's hydrophobicity, creating a droplet of the liquid on top of the electrodes, as shown in Figure 4.16, which would eventually pop draining all the dielectric already deposited. This behavior also made it complicated to ensure to fully cover the electrodes surface with the dielectric. With all this in mind, using the solid dielectric provided the best results for the fabrication of a functional supercapacitor. By being solid it also stays in the device without a need of enclosure, whereas the liquid one evaporates with time, making the device less durable.

Figure 4.16 - Hydrophobicity shown by the printed electrodes.

4.4.3 Geometry Influence

The supercapacitors geometry is a factor with a huge impact on the device's capacitance, since active area for charges storage should be optimized against the total area of the electrodes. The two geometries tested were printed, and the cyclic voltammetry curves were plotted, as showed in Figure 4.17. The CV curves from all the samples produced can be found in figure C3 to Figure C11 in annex C.

Comparing the plotted values of both geometries, it is possible to see that the planar geometry reaches current levels a lot higher than the interdigital one. Indeed, although the quantity of material used to print the electrodes is similar the active area between the electrodes is bigger in the planar geometry, 1cm^2 for the planar geometry and 0.26cm^2 for the interdigital.

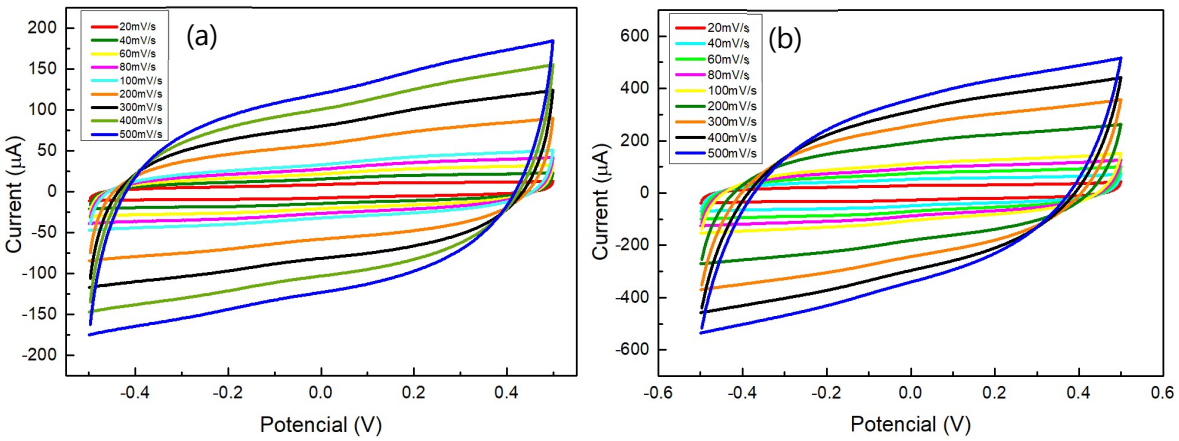

Figure 4.17 - Cyclic voltammetry curves of the two geometries tested (a) interdigital (sample 1i) and (b) planar (sample 1p).

Both devices display a stable behavior with a very symmetric rectangular-like shape, even at high scan rates, demonstrating an excellent capacitive behavior and rate performance. No redox peaks existed in the CV curves, indicating that the electrodes offer an excellent electrochemical stability.

At lower scan rates, the ions in the dielectric have enough time do diffuse into the graphene layers resulting in a higher specific capacitance. Figure 4.18 shows that as scan rate increases, the charge and discharge process is too quick to allow full ion diffusion, meaning less surface of the electrode is used resulting in a lower specific capacitance.

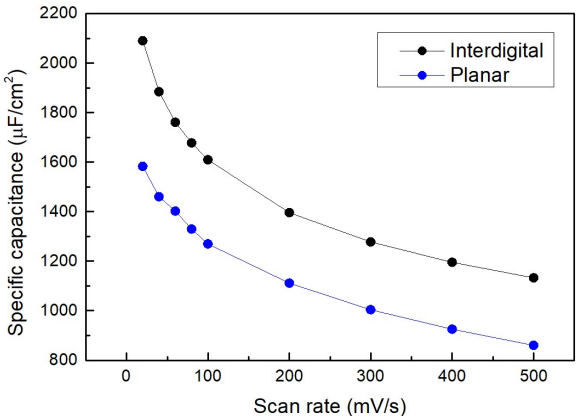

Figure 4.18 - Test results of the specific capacitance for the geometries tested at different scan rates

4.4.4 Electrochemical impedance spectroscopy

Electrochemical impendence spectroscopy is an important characterization for supercapacitors since it allows to understand how the different components of the device affect its performance. A model describing the circuit equivalent of an EDLC was found in the literature and it was used for this analysis, such model is displayed in Figure 4.19. [42].

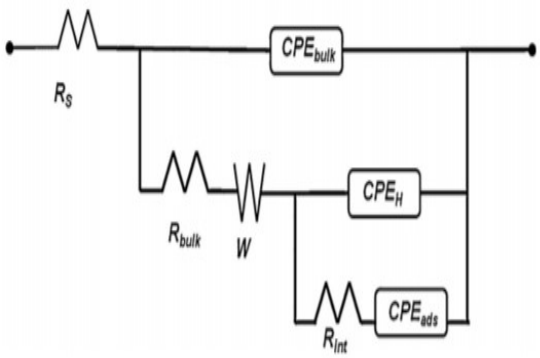

Figure 4.19 - Equivalent circuit modeling of the interfacial processes at the double layer and considering bulk processes. Adapted from [42].

Figure 4.20 shows the plotted values for the EIS characterization preformed on the supercapacitors with different geometries for frequencies between 10^{-2}Hz and 10^{-6}Hz. The capacitance seems to decrease proportionally with the frequency stabilizing as it reaches the lower frequencies which is an expected behavior for a supercapacitor.

The model used for the fitting on this test also seems to be the adequate one, since it has a goodness of fit in the magnitude of 10^{-6}, suggesting the devices fabricated exhibit an electrical double layer storage mechanism. The values of the parameters calculated by the model are displayed in Table B6 and Table B7 in annex B.

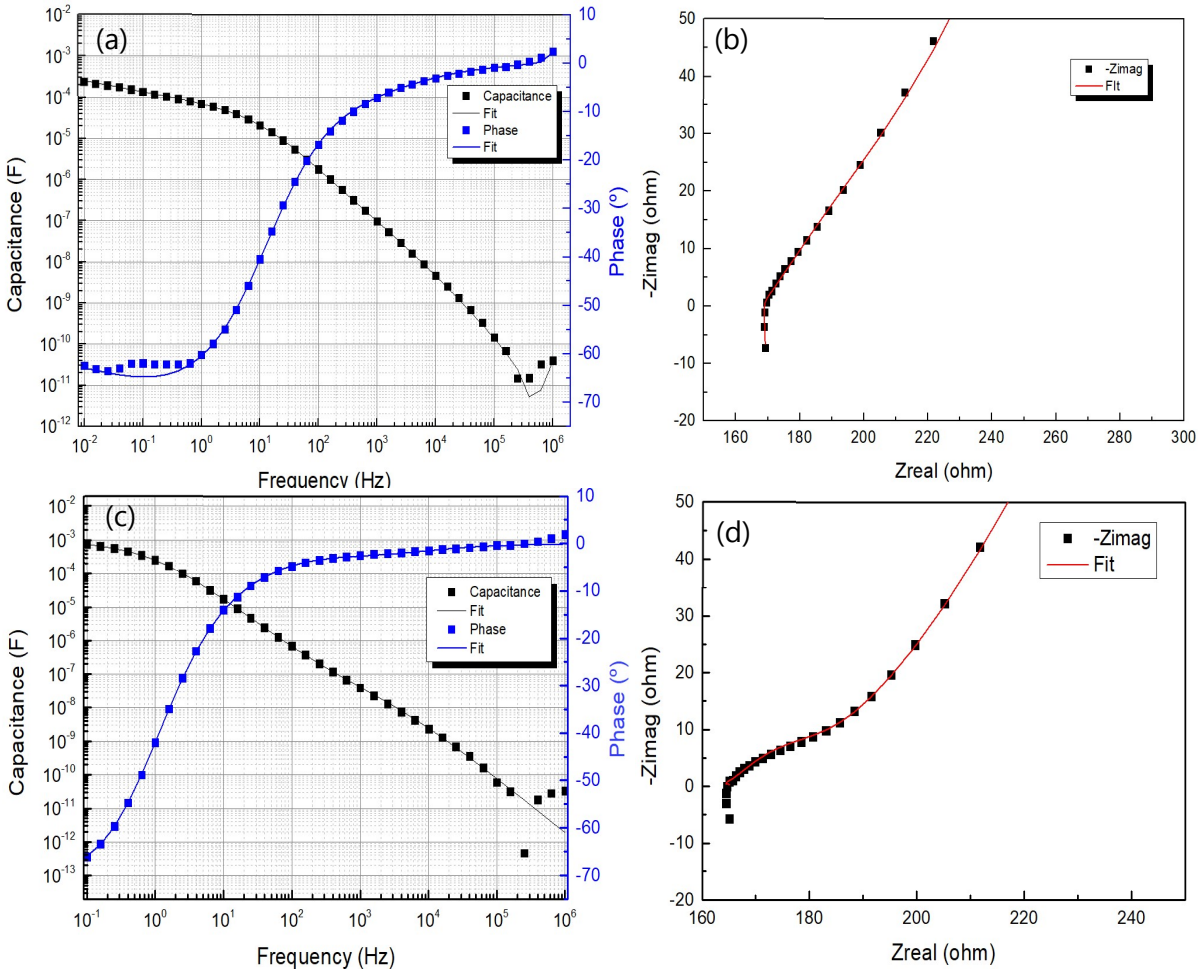

Figure 4.20 - (a) Bode and (b) Nyquist plots for the Interdigital geometry (sample 1i) and (c) Bode and (d) Nyquist plot for the planar geometry (sample 1p) using the fitting model found in literature [42].

4.4.5 Charge/discharge cycle stability

Devices such as supercapacitors must be able to keep a stable behavior throughout its use, meaning the device's capacitance needs to keep the properties after a considerable number of cycles. The already tested supercapacitors were submitted to 1000 cyclic voltammetry cycles followed by1000 more of chronoamperometry to understand how it behaved. The CV was done in a potential range between –0.5V and 0.5V with a scan rate of 100mV/s, and the cycles 1, 100, 500 and 1000 were plotted in Figure 4.22 and show that the symmetric rectangular-like shape was kept constant over the cycles.

This means the device's capacitance had no big variations, however this type of characterization is not very precise to study the capacitance variation and so the 1000 chronoamperometry cycles were performed on the same devices. Figure 4.22 shows the variation of the capacitance along the charge and discharge cycles, the current and potential variations through time for cycles 800, 801 and 802 are displayed in Figure 4.21.

The capacitance of the planar geometry seems to gradually drop until it reaches 200 cycles, and so it starts to stabilize at values between 2.5mF and 3mF. Furthermore, the current values for each cycle vary between −100μA and 100μA, and the potential has a variation expected from a supercapacitor, adopting a triangular shape.

The capacitance obtained for the interdigital geometry shows a higher deviation between cycles values, however the values constantly drop until it reaches 200 cycles, and it starts to stabilize 0.3mF and 0.6mF. Between cycles 250 and 750 some cycles appear to produce significantly higher capacitance values than what is expected, and the reason for that is unknown but it may be related to the electrolyte exposure to the atmosphere resulting in unforeseen reactions. The current and potential variations through time show a curve close to a triangular shape, confirming the formation of an efficient electrical double layer and a good charge propagation across the two electrodes.

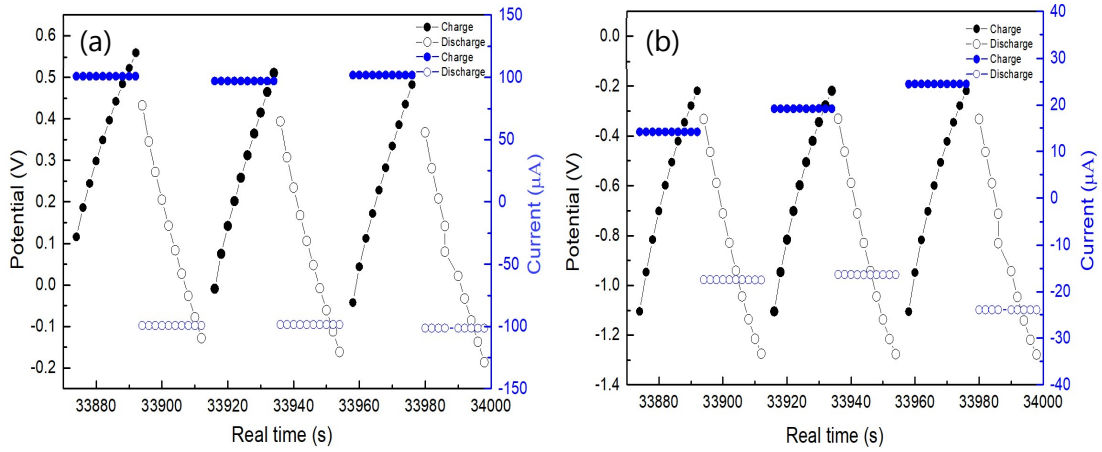

Figure 4.21 - Current and potential variations through charge and discharge cycles 800, 801 and 802 for the (a) planar (sample 1p) and (b) interdigital geometry (sample 8i).

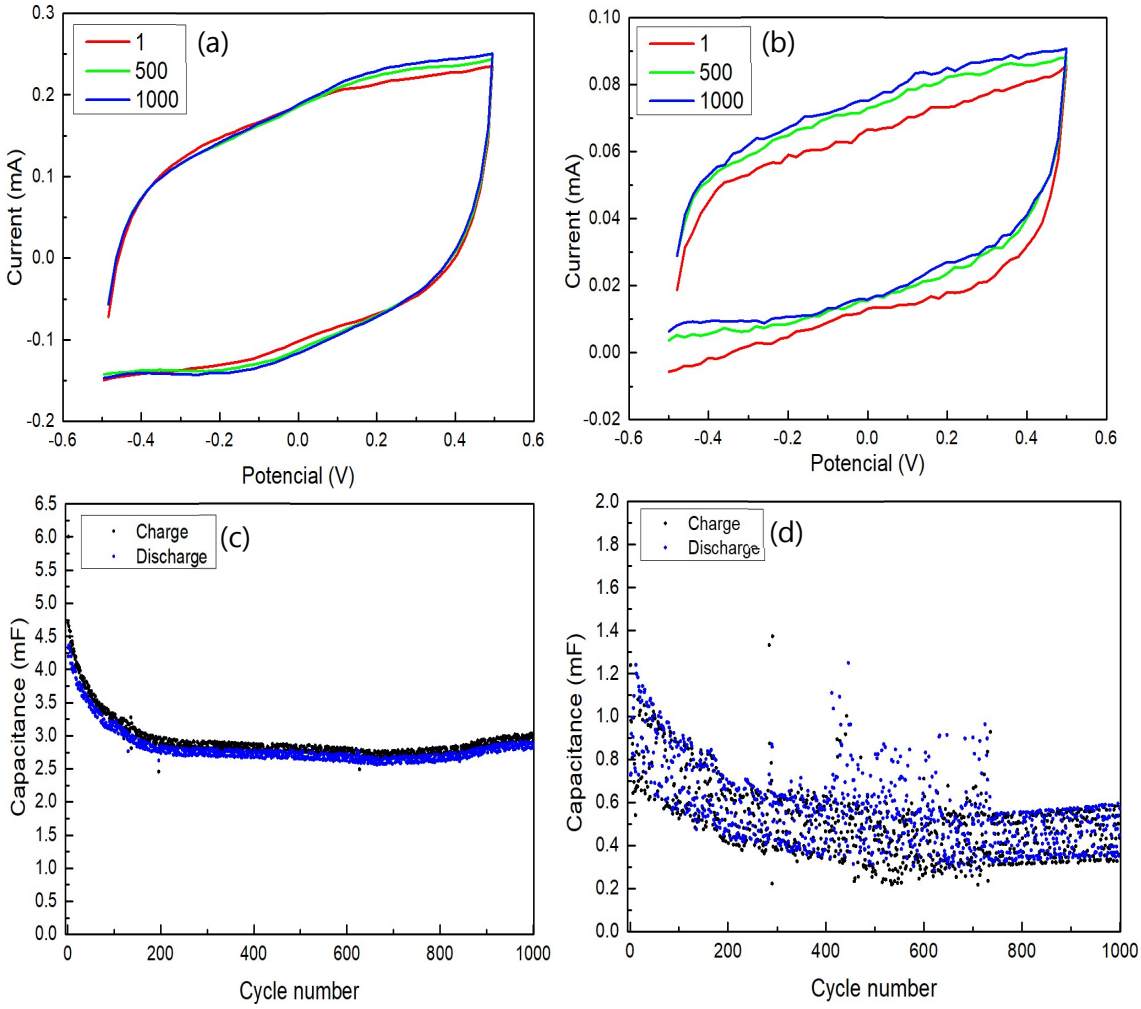

Figure 4.22 - 1000 cycles of cyclic voltammetry performed on (a) planar (sample 1p) and (b) Interdigital geometries (sample 8i), and 1000 charge/discharge cycles performed on the same (c) planar and (d) Interdigital geometries devices.

Overall, it is safe to say the devices fabricated behave like a supercapacitor and are stable even after more than 1000 cycles. The planar geometry had a more stable behavior and produced higher current and capacitance values. The Interdigital geometry should be further studied with a better encapsulation for better understanding of its behavior.

4.4.6 Device's time stability

Due to expected stability from the devices, they were kept in storage in room air conditions and re-measured after 1 month and 2 months, and results are displayed in Figure 4.23. The device used for this study had an interdigital geometry.

After 1 week of the device's production, the CV curve shows an oxidation peak and no apparent reduction peak, implying a none reversible redox reaction occurred (Figure 4.23 a). After 1 month however, the oxidation peak disappeared, and the voltammetry

geometry acquired a more defined rectangular-like shape with higher current values and maintaining this behavior after 2 months.

The device's specific capacity progression follows an asymptotic exponential growth with almost a 70% capacitance increase after 2 months of its fabrication.

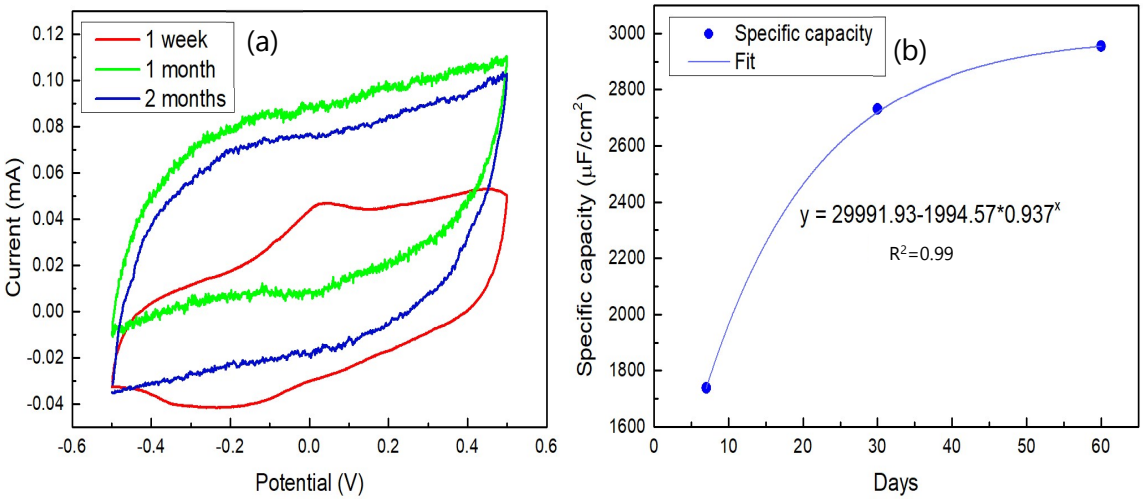

Figure 4.23 - Behavior progression of the supercapacitors produced for 2 months. (a) CV curve and (b) capacitance's progression.

This improvement maybe related to the electrolyte high viscosity that, has time passes after its deposition, gradually migrates more deeply into the electrode's pores making more contact with the surface increasing the active storage area.

.

5

5. Conclusion and future

The objectives of the thesis were successfully achieved. GO powder was produced by electrochemical exfoliation with properties that allow its use in inks for 3D printing. The two parameters studied show no need of fine tuning and represent inconsequential changes between the samples, displaying little discrepancies in the Raman spectra. However, the process can still be explored to obtain higher quality graphene sheets in the powder. One of the process steps that can be improved is the powder washing, during which the powder that stayed on top and in the bottom of the flask was kept. This powder separation can be explained by different densities of the micro grains in the powder. By only removing the powder from the top, we are ensuring the micro grains are composed by smaller stacks of graphene sheets, and therefore, possess a higher quality. The impact of this change in the process should be further studied and a design of experiment could be conducted to analyze the interdependence of the parameters.

It was also possible to manufacture 3D printable inks using the GO powder by mixing it with a binding agent. The choice of other binding agents may enable enchanting electrical conductivity, and therefore there could be other options that would yield better physical properties electrodes. Although the printed electrodes had acceptable conductive properties, the physical properties lacked elasticity leading the pieces to crack without a solid substrate, like glass. Different binding agents must be tested to optimize the ink's mechanical and electrical properties and print electrodes that do not require a solid substrate. Binding agents such as Hydroxy propyl methyl cellulose (HPMC) [43] and Carboxymethyl cellulose (CMC) [44] have proven to be a good alternative for extrusion based 3D printing inks, granting good mechanical properties to the pieces printed

From the two dielectrics analyzed, the solid one composed of PVA and diluted sulfuric acid showed to greatly increase the device's capacitance and to improve its electrical behavior, generating constant rectangular-like CV curves. This substance also proved to improve the device's behavior as it dried, which is a desired property. The sweat similar substance proved to be ineffective to fully cover the electrodes surface, making the

effective area used for charges storage smaller affecting drastically the device's specific capacitance.

Both device's geometries studied display conclusive results in its capacitance and durability. The planar geometry showed the lowest specific capacitance of the two and uses a lot more material, however it revealed to be as durable and stable as the interdigital geometry. For additional studies, testing a stacking approach using printed electrodes intercalated with the dielectric material could prove to be beneficial for the device's specific capacitance.

The capacitance values of the devices fabricated are comparable to supercapacitors technology at the same development stage, as seen in table B8 in annex B, meaning this low-cost process can still be improved for higher capacitance values.

The initial objectives of this work were accomplished. The devices were fabricated using a printable ink with GO powder, through an addictive manufacturing technique creating an all-solid-state supercapacitor with plenty of room to be optimized with a specific capacity of ~2mF/cm^2, stable for more than one month when stored at atmospheric conditions, with a decay capacitance less than 60% over more than 2000cycles.

6. Bibliography

[1] A. González, E. Goikolea, J. A. Barrena, and R. Mysyk, "Review on supercapacitors: Technologies and materials," *Renewable and Sustainable Energy Reviews*. 2016.

[2] Y. Huang, J. Liang, and Y. Chen, "An overview of the applications of graphene-based materials in supercapacitors," *Small*, vol. 8, no. 12, pp. 1805–1834, 2012.

[3] M. Vangari, T. Pryor, and L. Jiang, "Supercapacitors: Review of Materials and Fabrication Methods," *J. Energy Eng.*, 2012.

[4] I. Childres, L. Jauregui, W. Park, H. Cao, and Y. Chen, "Raman Spectroscopy of Graphene and Related Materials," *New Dev. Phot. Mater. Res.*, 2013.

[5] M. J. Allen, V. C. Tung, and R. B. Kaner, "Honeycomb carbon: A review of graphene," *Chem. Rev.*, 2010.

[6] Y.-H. Lin, C.-Y. Yang, S.-F. Lin, and G.-R. Lin, "Triturating versatile carbon materials as saturable absorptive nano powders for ultrafast pulsating of erbium-doped fiber lasers," *Opt. Mater. Express*, 2015.

[7] R. S. Shishir and D. K. Ferry, "Intrinsic mobility in graphene," *J. Phys. Condens. Matter*, 2009.

[8] Y. Zhu *et al.*, "Graphene and graphene oxide: Synthesis, properties, and applications," *Adv. Mater.*, 2010.

[9] F. Yavari and N. Koratkar, "Graphene-based chemical sensors," *Journal of Physical Chemistry Letters*. 2012.

[10] J. Zhu, D. Yang, Z. Yin, Q. Yan, and H. Zhang, "Graphene and graphene-based materials for energy storage applications," *Small*. 2014.

[11] Q. Zhou, X. Ye, Z. Wan, and C. Jia, "A three-dimensional flexible supercapacitor with enhanced performance based on lightweight, conductive graphene-cotton fabric electrode," *J. Power Sources*, 2015.

[12] R. Muñoz and C. Gómez-Aleixandre, "Review of CVD synthesis of graphene," *Chem. Vap. Depos.*, vol. 19, no. 10–12, pp. 297–322, 2013.

[13] K. S. Novoselov *et al.*, "Electric field in atomically thin carbon films," *Science (80-.).*, 2004.

[14] S. Gilje, S. Han, M. Wang, K. L. Wang, and R. B. Kaner, "A chemical route to graphene for device applications," *Nano Lett.*, 2007.

[15] B. C. Brodie, "the atomic weight of graphite," *Phil. Trans. R. Soc. Lond.*, 1859.

[16] C. Hontoria-Lucas, A. J. López-Peinado, J. de D. López-González, M. L. Rojas-Cervantes, and R. M. Martín-Aranda, "Study of oxygen-containing groups in a series of graphite oxides: Physical and chemical characterization," *Carbon N. Y.*, 1995.

[17] W. S. Hummers and R. E. Offeman, "Preparation of Graphitic Oxide," *J. Am. Chem. Soc.*, 1958.

[18] D. A. Dikin *et al.*, "Preparation and characterization of graphene oxide paper," *Nature*, 2007.

[19] J. Kauppila, P. Kunnas, P. Damlin, A. Viinikanoja, and C. Kvarnström, “Electrochemical reduction of graphene oxide films in aqueous and organic solutions,” *Electrochim. Acta*, 2013.

[20] J. I. Paredes and J. M. Munuera, “Recent advances and energy-related applications of high quality/chemically doped graphenes obtained by electrochemical exfoliation methods,” *J. Mater. Chem. A*, vol. 5, no. 16, pp. 7228–7242, 2017.

[21] W. Wu, C. Zhang, and S. Hou, “Electrochemical exfoliation of graphene and graphene-analogous 2D nanosheets,” *Journal of Materials Science*. 2017.

[22] S. Pei and H. Cheng, “The reduction of graphene oxide,” *Carbon N. Y.*, vol. 50, no. 9, pp. 3210–3228, 2011.

[23] V. Singh, D. Joung, L. Zhai, S. Das, S. I. Khondaker, and S. Seal, “Graphene based materials: Past, present and future,” *Prog. Mater. Sci.*, vol. 56, no. 8, pp. 1178–1271, 2011.

[24] Marin S. Halper James C. Ellenbogen, “Supercapacitors: A Brief Overview,” *Biosens. Bioelectron.*, vol. 25, no. 7, pp. 1629–1634, 2010.

[25] M. Winter and R. J. Brodd, “What are batteries, fuel cells, and supercapacitors?,” *Chem. Rev.*, 2004.

[26] A. M. Namisnyk, “A Survey of Elctrochemical Supercapacitor Technology,” *Electr. Eng.*, 2003.

[27] L. L. Zhang, R. Zhou, and X. S. Zhao, “Graphene-based materials as supercapacitor electrodes,” *J. Mater. Chem.*, vol. 20, no. 29, pp. 5983–5992, 2010.

[28] R. Raccichini, A. Varzi, S. Passerini, and B. Scrosati, “The role of graphene for electrochemical energy storage,” *Nat. Mater.*, 2015.

[29] M. Conway *et al.*, “Ultrathin Planar Graphene Supercapacitors,” *Nano Lett.*, vol. 11, no. 4, pp. 1423–1427, 2011.

[30] P. L. Huang *et al.*, “Ionic liquid electrolytes with various constituent ions for graphene-based supercapacitors,” *Electrochim. Acta*, 2015.

[31] Z. Niu, L. Zhang, L. Liu, B. Zhu, H. Dong, and X. Chen, “All-solid-state flexible ultrathin micro-supercapacitors based on graphene,” *Adv. Mater.*, 2013.

[32] T. D. Ngo, A. Kashani, G. Imbalzano, K. T. Q. Nguyen, and D. Hui, “Additive manufacturing (3D printing): A review of materials, methods, applications and challenges,” *Compos. Part B Eng.*, vol. 143, no. February, pp. 172–196, 2018.

[33] S. Naficy *et al.*, “Graphene oxide dispersions: Tuning rheology to enable fabrication,” *Mater. Horizons*, 2014.

[34] K. Fu *et al.*, “Graphene Oxide-Based Electrode Inks for 3D-Printed Lithium-Ion Batteries,” *Adv. Mater.*, vol. 28, no. 13, pp. 2587–2594, 2016.

[35] G. Xin *et al.*, “Highly thermally conductive and mechanically strong graphene fibers,” *Science (80-.).*, vol. 349, no. 6252, pp. 1083–1087, 2015.

[36] C. Callewaert, B. Buysschaert, E. Vossen, V. Fievez, T. Van de Wiele, and N. Boon, “Artificial sweat composition to grow and sustain a mixed human axillary microbiome,” *J. Microbiol. Methods*, 2014.

[37] X. Ding *et al.*, “Spinning fabrication of graphene/polypyrrole composite fibers for all-

solid-state, flexible fibriform supercapacitors," *J. Mater. Chem. A*, vol. 2, no. 31, pp. 12355–12360, 2014.

[38] K. Krishnamoorthy, M. Veerapandian, K. Yun, and S. J. Kim, "The chemical and structural analysis of graphene oxide with different degrees of oxidation," *Carbon N. Y.*, vol. 53, pp. 38–49, 2013.

[39] K. Narinder, *Comprehensive Physics for Class XII*. New delhi: Laxmi Publications, 2003.

[40] Z. W. Ouyang, E. C. Chen, and T. M. Wu, "Thermal stability and magnetic properties of polyvinylidene fluoride/magnetite nanocomposites," *Materials (Basel).*, vol. 8, no. 7, pp. 4553–4564, 2015.

[41] S. B. Aziz, T. J. Woo, M. F. Z. Kadir, and H. M. Ahmed, "A conceptual review on polymer electrolytes and ion transport models," *J. Sci. Adv. Mater. Devices*, vol. 3, no. 1, pp. 1–17, 2018.

[42] J. Kang, J. Wen, S. H. Jayaram, A. Yu, and X. Wang, "Development of an equivalent circuit model for electrochemical double layer capacitors (EDLCs) with distinct electrolytes," *Electrochim. Acta*, vol. 115, pp. 587–598, 2014.

[43] U. K. Roopavath, S. Malferrari, A. Van Haver, F. Verstreken, S. N. Rath, and D. M. Kalaskar, "Optimization of extrusion based ceramic 3D printing process for complex bony designs," *Mater. Des.*, vol. 162, pp. 263–270, 2019.

[44] G. Zheng, L. Hu, H. Wu, X. Xie, and Y. Cui, "Paper supercapacitors by a solvent-free drawing method," *Energy Environ. Sci.*, vol. 4, no. 9, pp. 3368–3373, 2011.

7. Annexes

Annex A

Figure A1 - Powder produced with 0.5M of H_2SO_4 and applying a 10V potential.

Figure A2 - Powder produced with 0.2M of H_2SO_4 and applying a 10V potential.

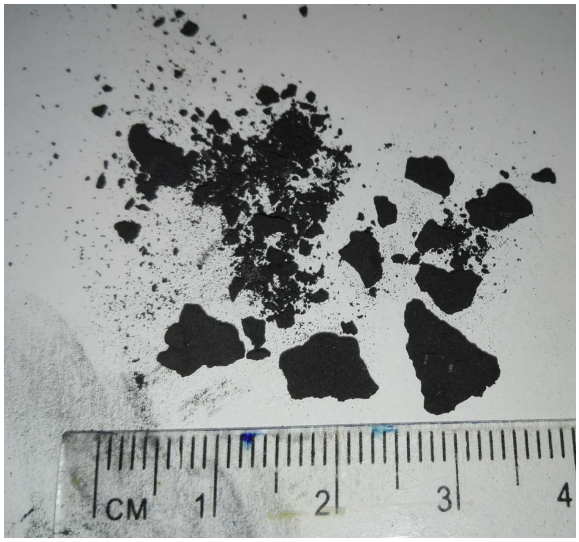

Figure A3 - Powder produced with 1M of H_2SO_4 and applying a 10V potential.

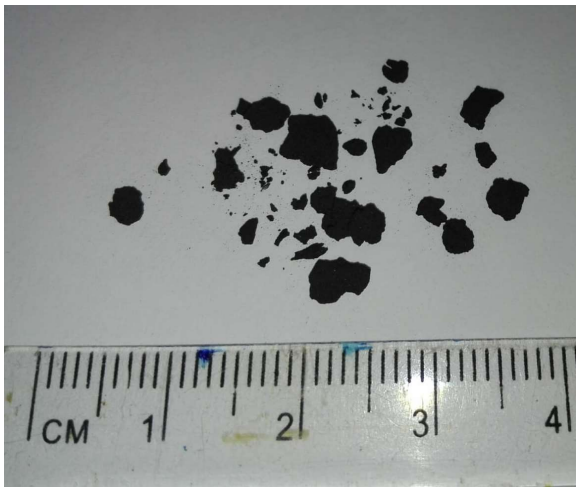

Figure A4 - Powder produced with 0.2M of H_2SO_4 and applying a 13V potential.

Figure A5 - 3D printed supercapacitors samples. Displayed, from left to right are samples 1i, 2i, 3i, 4i and 5i.

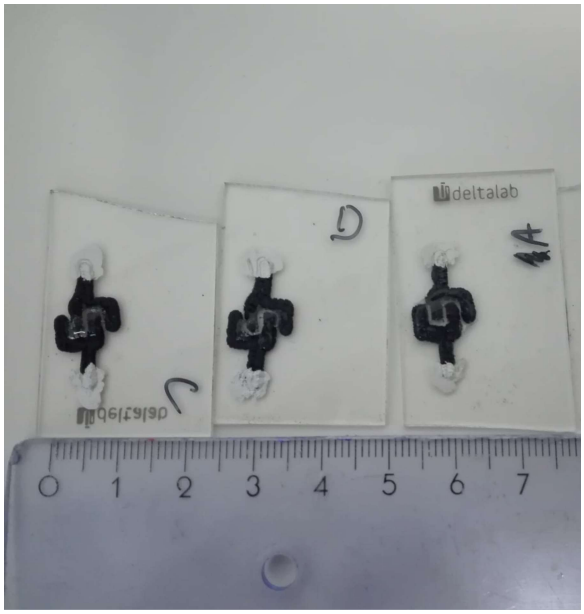

Figure A6 - 3D printed supercapacitors samples. Displayed, from left to right are samples 6i, 7i, 8i.

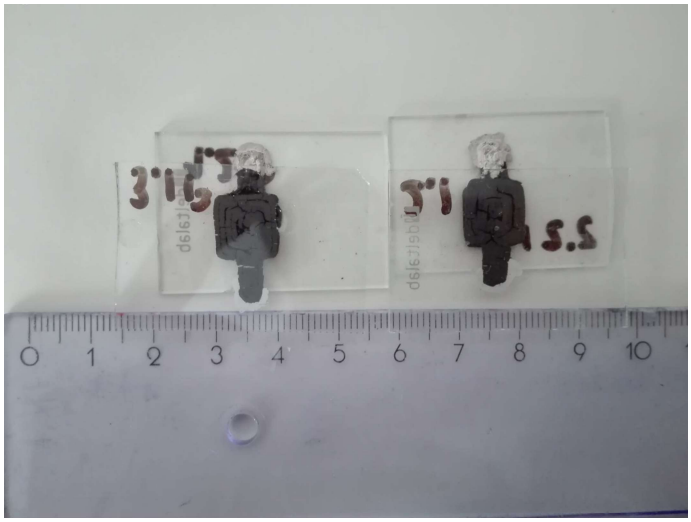

Figure A7 - 3D printed supercapacitors samples. Displayed, from left to right are samples 2p and 1p.

Annex B

Table B1 - Samples used for the determination of the mean resistance of each ink produced with different GO concentrations.

GO concentration (%)	Resistivity (ohm.cm)	Mean value	Standard deviation
73	0.11	0.13	0.02
73	0.16		
73	0.13		
75	0.16	0.22	0.08
75	0.31		
75	0.20		
80	0.28	0.30	0.20
80	0.30		
80	0.32		

Table B2 - Samples used for the determination of the mean resistance of the samples heat treated with different atmospheres.

Atmos-phere	Resistivity (ohm.cm)	Mean Value	Standard deviation
Nitrogen	3.60	55.596	4.551
	5.47		
	5.87		
Oxygen	50.87	4.979	1.209
	59.95		
	55.96		
Vacuum	24.59	26.249	2.179
	28.72		
	25.45		

Table B3 - Samples used for the determination of the mean resistance for each heat treatment at different temperatures under nitrogen atmosphere.

Temperature (°C)	Resistivity (ohm.cm)	Mean Value	Standard deviation
100	353.86	353.82	2.28
	356.08		
	351.52		
150	182.46	182.14	2.42
	184.39		
	179.57		
200	53.95	54.28	1.55
	52.92		
	55.98		
270	32.61	32.50	1.90
	30.54		
	34.34		
320	3.60	4.98	1.21
	5.47		
	5.86		

Table B4 - Samples used for the determination of the mean resistance used for the study of the surfactant concentration influence.

Surfactant concentration (µL/mL)	Resistivity (ohm.cm)	Mean value	Standard deviation
0	3.57	4.68	1.15
	5.87		
	4.60		
2	103.86	133.99	26.21
	151.45		
	146.67		
5	130.10	127.09	6.87
	131.94		
	119.22		
8	214.18	323.28	154.29
	432.38		

Table B5 - Best printing parameters determined for GO/PVDF/DMF ink by trial and error.

Nozzle diameter (mm)	Extrusion multiplier	First layer height (%)	First layer speed (%)	Primary layer height (mm)	Interior fill percentage (%)	Default printing speed (mm/min)	X/Y axis movement speed (mm/min)	Filament diameter (mm)
0.7	20	100	70	0.5	100	400	800	0.9

Table B6 - Parameters obtained by the fitting model found in the literature for the Interdigital geometry

Parameter	Value	± error	Units
Rs	168.2	7.913	ohm
Rbulk	-6,66E-01	2.682	ohm
CPEbulk	76.51e-6	36.62e-6	S*s^a
a24	624.0e-3	58.14e-3	
W25	409.3e-6	118.3e-6	S*s^(1/2)
Rint	75.02	85.65	ohm
CPEh	-2,27E-03	40.10e-6	S*s^a
a28	812.1e-3	1.136	
CPEads	71.25e-6	14.93e-6	S*s^a
a30	926.5e-3	65.69e-3	
Goodness of Fit	535.7e-6		

Table B7 - Parameters obtained by the fitting model found in the literature for the planar geometry

Parameter	Value	± error	Units
Rs	164.9	3.267	ohm
Rbulk	21.76	23.78	ohm
CPEbulk	107.7e-6	523.9e-6	S*s^a
a24	644.2e-3	470.5e-3	
W25	2,13E+00	881.3e-6	S*s^(1/2)
Rint	-1,35E+06	39.97e3	ohm
CPEh	827.2e-6	763.9e-6	S*s^a
a28	1.000	398.3e-3	
CPEads	114.3e-6	1,45E+00	S*s^a
a30	443.5e-3	2.870	
Goodness of Fit	63.12e-6		

Table B8- Comparison between the specific capacitance from various carbon-based supercapacitors

Component	Capacitance ($\mu F/cm^2$)	Reference
Basal plane of stress-annealed pyrolytic graphite	3-4	(1)
Graphene prepared by nanodiamond route	6.7	(2)
Graphene prepared by exfoliation	12.4	(2)
3D Printed Graphene Based Supercapacitors	1062 - 6399	
Paper supercapacitors by solvent-free drawing method	2300	(3)

(1) J.-P. Randin and E. Yeager, "Differential capacitance study on the basal plane of stress-annealed pyrolytic graphite," *J. Electroanal. Chem. Interfacial Electrochem.*, vol. 36, no. 2, pp. 257–276, May 1972.

(2) P. Hiralal, G. Rius, M. Yoshimura, and G. A. J. Amaratunga, "Graphene-based electrochemical capacitors," *Graphene Sci. Handb. Size-Dependent Prop.*, vol. 120, no. 1, pp. 479–494, 2016.

(3) G. Zheng, L. Hu, H. Wu, X. Xie, and Y. Cui, "Paper supercapacitors by a solvent-free drawing method," *Energy Environ. Sci.*, vol. 4, no. 9, pp. 3368–3373, 2011.

Annex C

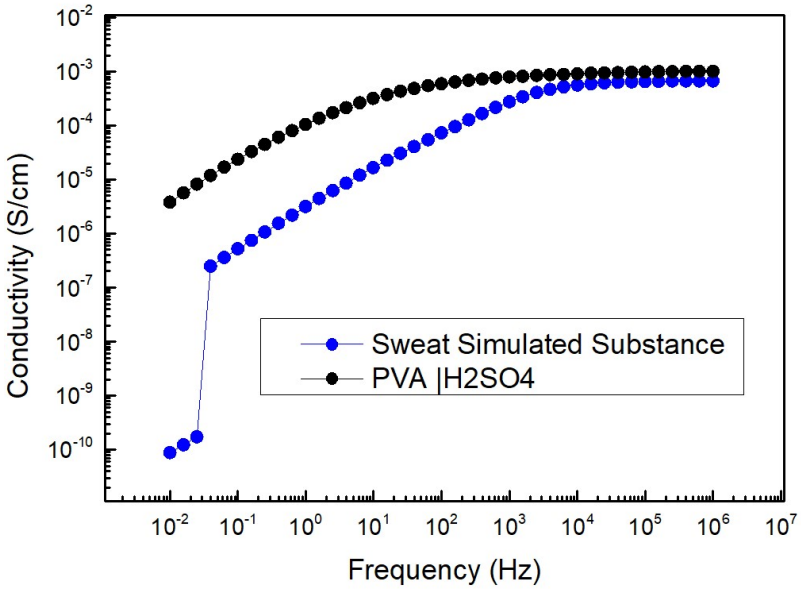

Figure C1 - Electrical conductivity variation with frequency for sample 7i.

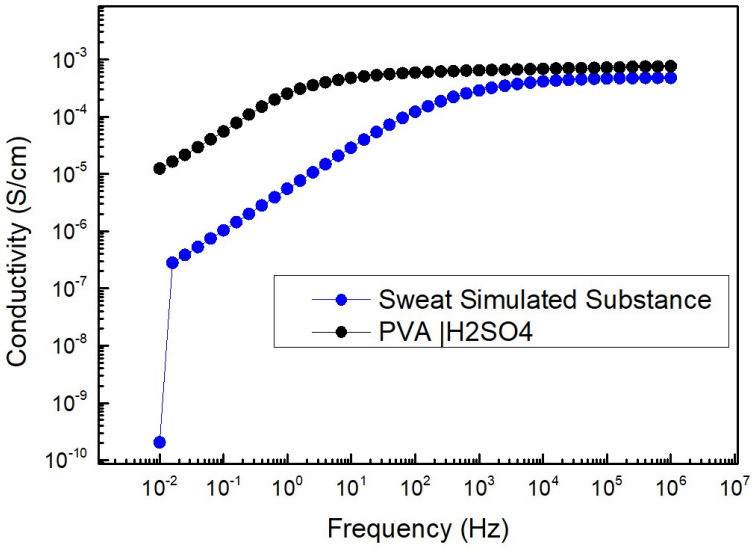

Figure C2 - Electrical conductivity variation with frequency for sample 8i.

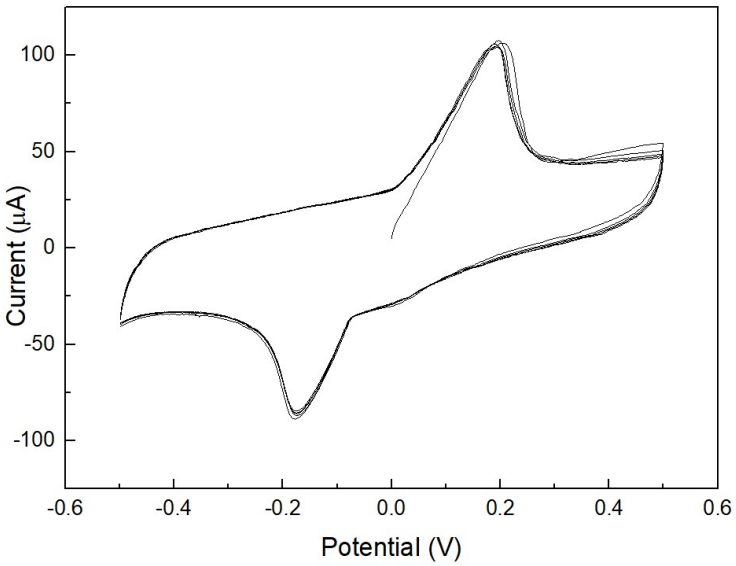

Figure C3 - CV curve from sample 2i with PVA/H_2SO_4 as an electrolyte, between -0.5V and 0.5V at 60mV/s with an interdigital geometry. 5 cycles are represented.

Sample 2i had a connection between the silver ink contacts and the electrolyte deposited, which may be the reason why there is a reversible redox reaction. On this device were performed 20 cycles to see If the peaks disappeared but the device's behavior kept constant and similar to the one displayed in Figure C2.

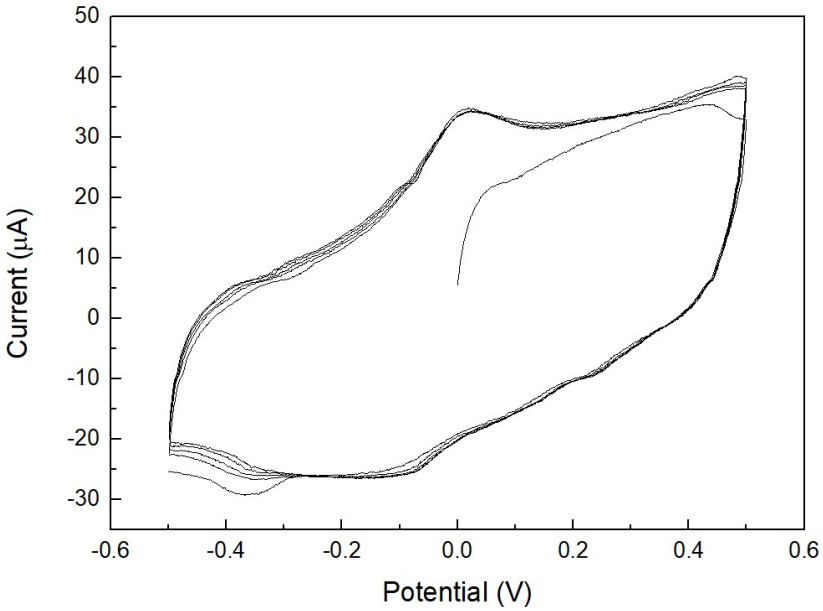

Figure C4 - CV curve from sample 3i with PVA/H_2SO_4 as an electrolyte, between -0.5V and 0.5V at 60mV/s with an interdigital geometry. 5 cycles are represented.

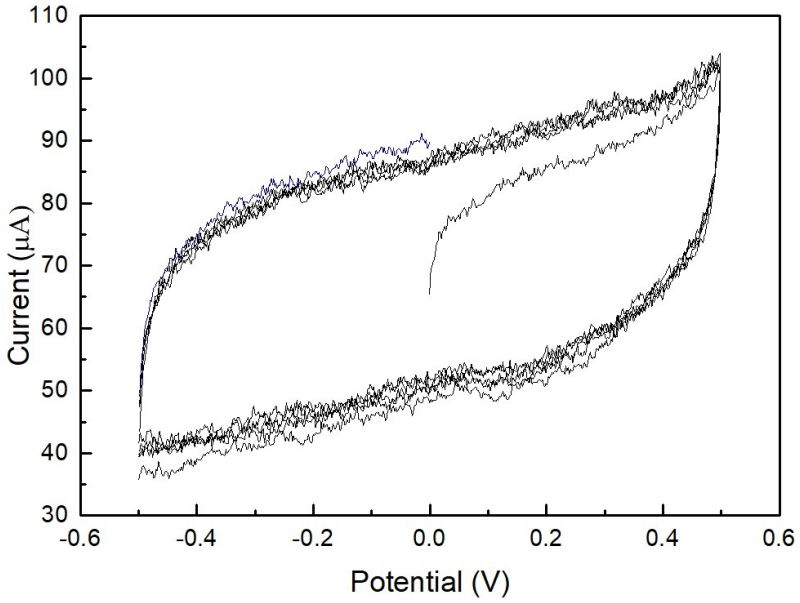

Figure C5 - CV curve from sample 4i with PVA/ H_2SO_4 as an electrolyte, between -0.5V and 0.5V at 60mV/s with an interdigital geometry. 5 cycles are represented.

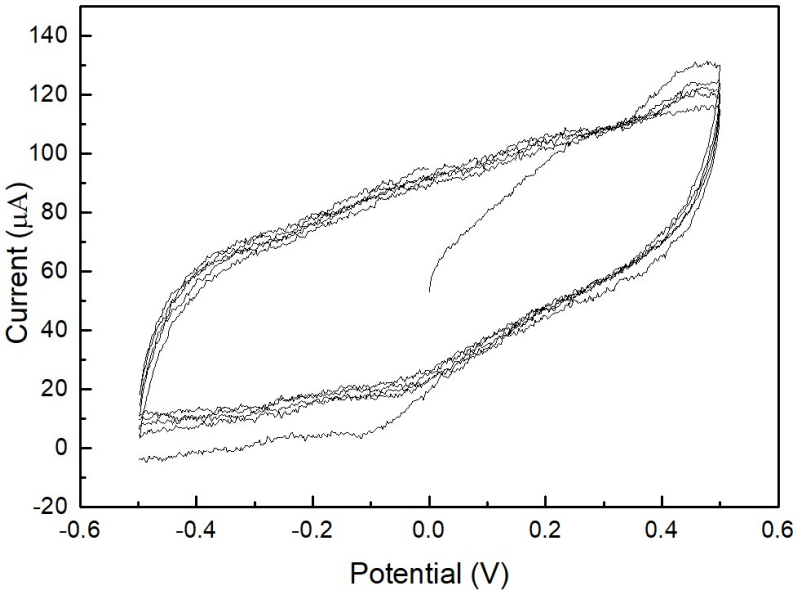

Figure C6 - CV curve from sample 5i with PVA/H_2SO_4 as an electrolyte, between -0.5V and 0.5V at 60mV/s with an interdigital geometry. 5 cycles are represented.

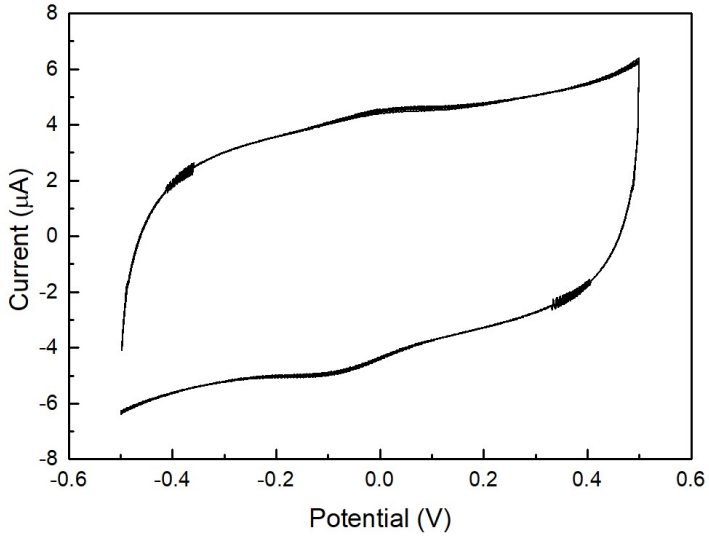

Figure C7 - CV curve from sample 6i with PVA/H_2SO_4 as an electrolyte, between -0.5V and 0.5V at 60mV/s with an interdigital geometry. 5 cycles are represented.

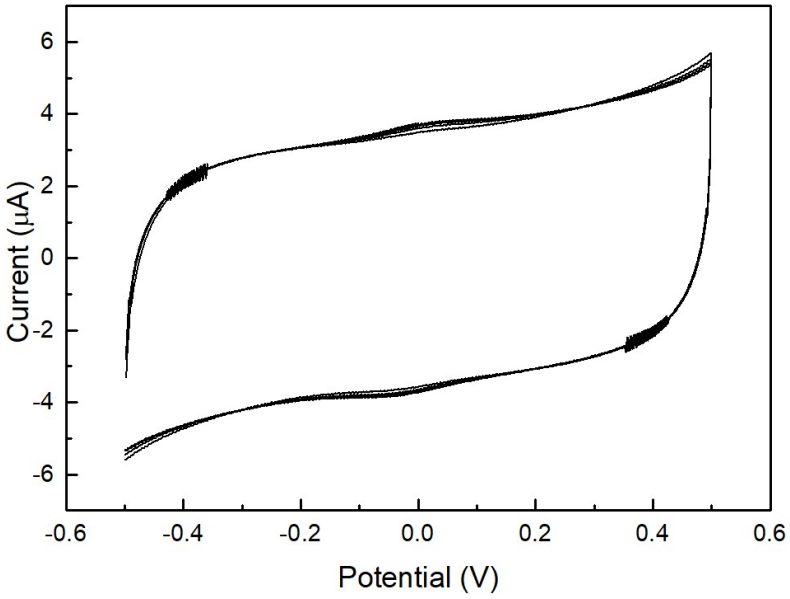

Figure C8 - CV curve from sample 7i with H_2SO_4 as an electrolyte, between -0.5V and 0.5V at 60mV/s with an interdigital geometry. 5 cycles are represented.

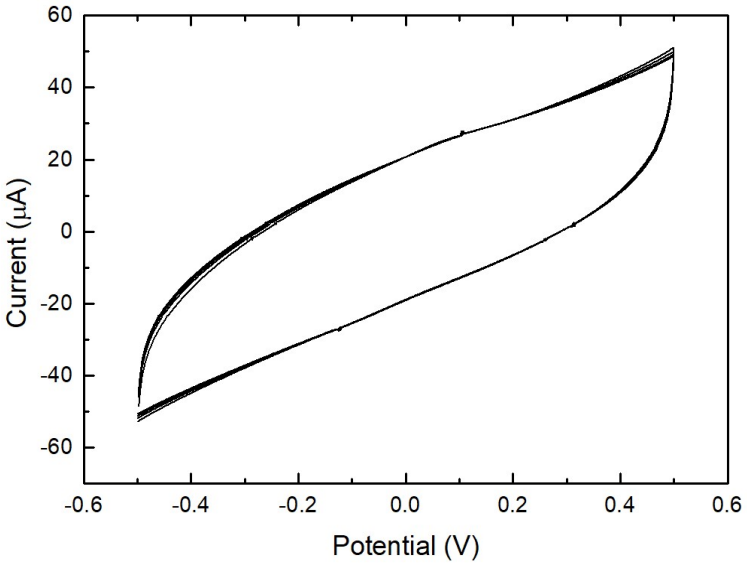

Figure C9 -CV curve from sample 8i with H_2SO_4 as an electrolyte, between -0.5V and 0.5V at 60mV/s with an interdigital geometry. 5 cycles are represented

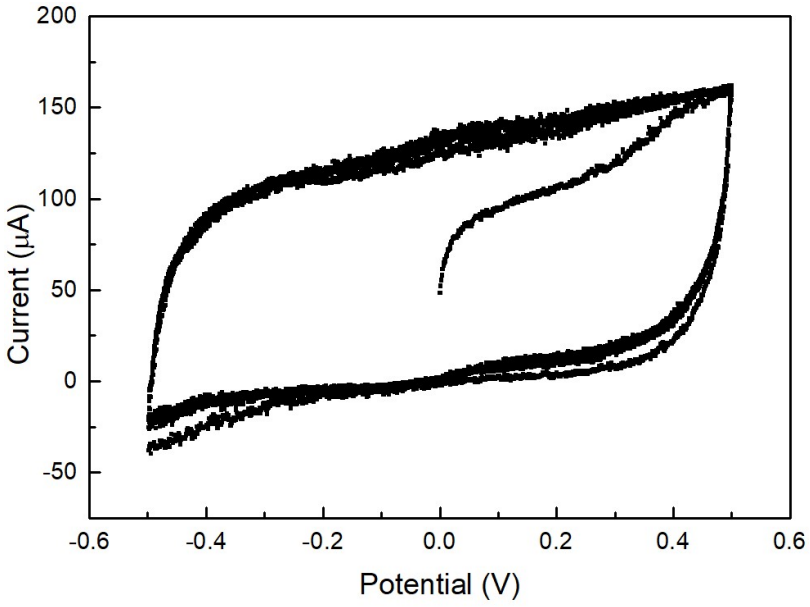

Figure C10 - CV curve from sample 1p with PVA/H_2SO_4 as an electrolyte, between -0.5V and 0.5V at 60mV/s with a planar geometry. 5 cycles are

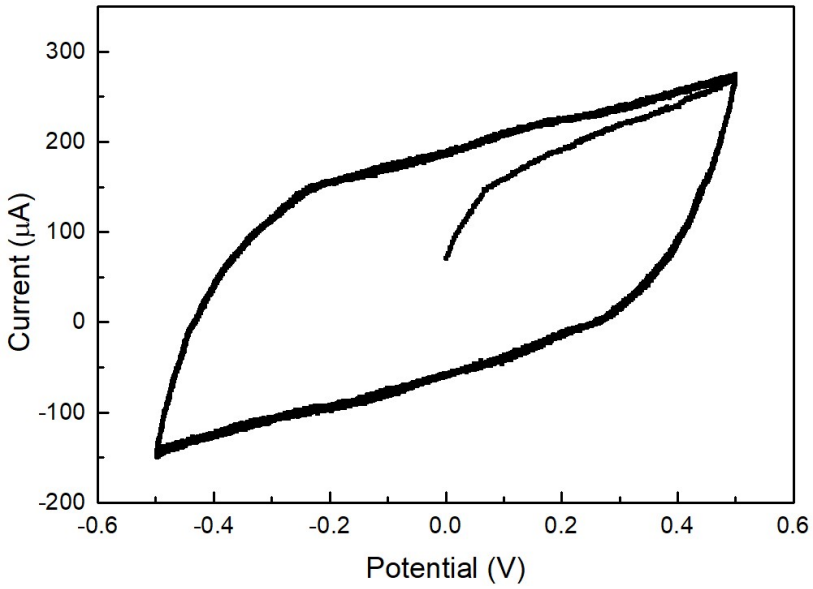

Figure C11 - CV curve from sample 2p with PVA/H_2SO_4 as an electrolyte, between -0.5V and 0.5V at 60mV/s with a planar geometry. 5 cycles are represented.